Supplement to "Metrology with $\mathcal{PT}$-symmetric cavities: Enhanced sensitivity near the $\mathcal{PT}$-phase transition"

This supplement provides detailed derivations of some equations given in the main text of the paper on the following topics: (I) Mechanism of amplification in $\mathcal{PT}$-symmetric metrology systems; (II) Amplification in a system with two coupled lossy cavities; (III) Amplification in a system with an active cavity; (IV) Phonon sidebands, and (V) Displacement spectral densities in the active cavity, $\mathcal{PT}$ and EP optomechanical transducer.

I. MECHANISM OF AMPLIFICATION IN $\mathcal{PT}$-SYMMETRIC METROLOGY SYSTEM

The non-Hermitian Hamiltonian of our $\mathcal{PT}$-symmetric metrology system can be written as

$$H = (\Delta - i\kappa)\, a^\dagger a + (\Delta + i\gamma)\, c^\dagger c + g_1(a^\dagger c + c^\dagger a) + g a^\dagger a z, \tag{1}$$

where a and c are, respectively, the annihilation operators of the lossy cavity (passive cavity) and the gain cavity (active cavity); κ and γ are the damping and gain rates of the two cavities. The coupling strength between the passive and active cavities is denoted by g_1, the coupling strength between the system and the passive cavity is given by g, and the effective frequencies of the two cavities are assumed to be as Δ (i.e., the solitary cavities are degenerate in their resonance frequencies).

The Hamiltonian in Eq. (1) without the term $ga^\dagger az$ (this term describes the interaction between the passive cavity and the system to be measured) describes the optical modes of the cavities and their interaction:

$$H_1 = (\Delta - i\kappa)\, a^\dagger a + (\Delta + i\gamma)\, c^\dagger c + g_1(a^\dagger c + c^\dagger a). \tag{2}$$

We consider the case in which gain and loss are balanced, i.e., $\Gamma = (\kappa + \gamma)/2 = \kappa$. In this case, the Hamiltonian in Eq. (2) can be rewritten in a matrix form as [1, 2]

$$H_1 = \begin{bmatrix} re^{i\theta} & g_1 \\ g_1 & re^{-i\theta} \end{bmatrix},$$

where $r = \sqrt{\Delta^2 + \kappa^2}$ and $\theta = \arctan(\kappa/\Delta)$. The eigenvalues of H can be written as $\lambda_\pm = r\cos\theta \pm \sqrt{g_1^2 - r^2\sin^2\theta}$, and the corresponding eigenvectors are

$$|E_+\rangle = \begin{pmatrix} e^{i\alpha/2} \\ e^{-i\alpha/2} \end{pmatrix}, \qquad |E_-\rangle = \begin{pmatrix} ie^{-i\alpha/2} \\ -ie^{i\alpha/2} \end{pmatrix},$$

where $\sin\alpha = (r\sin\theta)/g_1$.

The interaction Hamiltonian $H_{\rm int} = ga^\dagger az$ in Eq. (1) can be re-expressed in the supermode picture, under which we can find that the effective coupling strength between the supermodes and the system to be measured can be represented by

$$g_{\rm eff} = \frac{g\left(\Gamma + \sqrt{\Gamma^2 - g_1^2}\right)}{2\sqrt{\Gamma^2 - g_1^2}}. \tag{3}$$

In the vicinity of the transition point, which takes place at $g_1 = \Gamma$, we have $g_{\rm eff} \to \infty$; which implies that in such a case we have an extremely strong effective coupling $g_{\rm eff}$ between the supermodes $a_\pm$ and the measured observable z. This, in turn, leads to a sharp increase in the sensitivity of the measurement.

In order to clarify the underlying mechanism of the proposed $\mathcal{PT}$-induced highly-sensitive measurements, below we derive the expressions for the spectra of the output fields in both the $\mathcal{PT}$ symmetric regime and the broken-$\mathcal{PT}$ regime. Here, we assume that the gain of the active cavity is induced by the coupling between the cavity mode and an ensemble of atoms, thus the Hamiltonian of the total system can be written as

$$H = \Delta a^\dagger a + \Delta c^\dagger c + \frac{\omega_a}{2} J_z + g_1(a^\dagger c + c^\dagger a) + g_2(J_- c^\dagger + J_+ c) + g a^\dagger a z, \tag{4}$$

where ω_a is the effective frequency of the atomic ensemble, and g_2 is the effective coupling strength between the cavity mode and the atomic ensemble. By considering further the fluctuation terms which are induced by, e.g., the electrical noises or vacuum fluctuations, the equations of motion for the total system can be expressed as

$$\begin{aligned}
\dot{a} &= -i\Delta a - igaz - ig_1 c - \kappa a - \sqrt{2\kappa}a_{\rm in}, &(5)\\
\dot{c} &= -i\Delta c - ig_1 a - \kappa_c c - ig_2 J_- - \sqrt{2\kappa_c}c_{\rm in}, &(6)\\
\dot{J}_- &= -i\omega_a J_- - 2\gamma_0 J_- + ig_2 J_z c - \sqrt{2\gamma_0}J_z d_{\rm in}, &(7)\\
\dot{J}_z &= p - 2\gamma_1 J_z - i2g_2 J_+ c + i2g_2 J_- c^\dagger - 2\sqrt{2\gamma_1}J_+ d_{\rm in} - 2\sqrt{2\gamma_1}J_- d_{\rm in}^\dagger, &(8)
\end{aligned}$$

where J_- and J_z are the collective ladder and z-axis Pauli operators of the atomic ensemble; κ_c is the decay rate of the active cavity; p denotes the population inversion; and γ_0 and γ_1 are the effective dissipation and pure-dephasing rates of the atomic ensemble. The input field $a_{\rm in}$ fed into the passive cavity can be taken as a sum of a coherent input field with complex amplitude α and a white noise term $\xi(t)$, i.e., $a_{\rm in} = \alpha + \xi(t)$. In order to simplify our discussion, we assume that the fields $c_{\rm in}$ and $d_{\rm in}$ fed into the active cavity and the atomic ensemble are white noises. From Eq. (6) and Eq. (7), we can obtain the following equation for the cavity mode by eliminating the degrees of freedom of J_- by setting $\dot{J}_- = 0$,

$$\dot{c} = -i\Delta c - ig_1 a - \kappa_c c + \frac{g_2^2}{\gamma_0}J_z c - \sqrt{2\kappa_c}c_{\rm in} + i\frac{g_2^2}{\sqrt{\gamma_0}}J_z d_{\rm in}. \tag{9}$$

By adiabatically eliminating the degrees of freedom of the atomic ensemble, the dynamical equations of our $\mathcal{PT}$-symmetric metrology system can be expressed as

$$\begin{aligned}
\dot{a} &= -i\Delta a - igaz - ig_1 c - \kappa a - \sqrt{2\kappa}a_{\rm in},\\
\dot{c} &= -i\Delta c - ig_1 a + \gamma c - \sqrt{2\kappa_c}c_{\rm in} + iDd_{\rm in}, &(10)
\end{aligned}$$

where $\gamma = g_2^2 p/(\gamma_0\gamma_1) - \kappa_c$, and $D = g_2^2 p/(\sqrt{\gamma_0}\gamma_1)$. Using Parseval's theorem [3], we can write the power spectrum of the cavity field as $\tilde{S}(\omega) = |\tilde{A}(\omega)|^2$, where

$$\tilde{A}(\omega) = -\alpha F_2(\omega) - F_1(\omega)\int_{-\infty}^{+\infty} {\rm d}\omega_1 \tilde{A}(\omega_1) Z(\omega - \omega_1) \tag{11}$$

is the Fourier transform of the intracavity field of the passive cavity. Here, $F_1(\omega)$ and $F_2(\omega)$ are defined as

$$\begin{aligned}
F_1(\omega) &= \frac{[-\gamma + i(\Delta - \omega)]\, g}{g_1^2 + [-\gamma + i(\Delta - \omega)]\,[\kappa + i(\Delta - \omega)]}, &(12)\\
F_2(\omega) &= \frac{[-\gamma + i(\Delta - \omega)]\,\sqrt{2\kappa} - g_1 D + ig_1\sqrt{2\kappa_c}}{g_1^2 + [-\gamma + i(\Delta - \omega)]\,[\kappa + i(\Delta - \omega)]}, &(13)
\end{aligned}$$

and $Z(\omega)$ is the Fourier transform of the measured observable z. If gain and loss are balanced, in the vicinity of the transition point, we have

$$\frac{g_1 D}{\gamma\sqrt{2\kappa}} = \frac{p\sqrt{2\kappa\gamma_0}}{\gamma_1}. \tag{14}$$

Considering the case in which $p\sqrt{2\kappa\gamma_0} \ll \gamma_1$, we can neglect the term D in Eq. (13). Then, due to $\Delta\sqrt{2\kappa} \gg g_1\sqrt{2\kappa_c}$, $F_2(\omega)$ can be expressed as

$$F_2(\omega) = \frac{[-\gamma + i(\Delta - \omega)]\,\sqrt{2\kappa}}{g_1^2 + [-\gamma + i(\Delta - \omega)]\,[\kappa + i(\Delta - \omega)]}.$$

Iterating Eq. (11) by substituting the value of $\tilde{A}(\omega)$ at the frequency ω_1 into the integral term in Eq. (11), we can re-express Eq. (11) as

$$\begin{aligned}
\tilde{A}(\omega) &= -\alpha F_2(\omega) + \alpha F_1(\omega)\int_{-\infty}^{+\infty} {\rm d}\omega_1 F_2(\omega_1) Z(\omega - \omega_1)\\
&\quad + F_1(\omega)\int_{-\infty}^{+\infty} {\rm d}\omega_1 \int_{-\infty}^{+\infty} {\rm d}\omega_2 F_1(\omega_1)\tilde{A}(\omega_2) Z(\omega - \omega_1) Z(\omega_1 - \omega_2). &(15)
\end{aligned}$$

Doing the same iteration further using the value of $\tilde{A}(\omega)$ at many other frequencies $\omega_2, \ldots, \omega_n$, we can write $\tilde{A}(\omega)$ as infinite series of the form

$$\begin{aligned}\tilde{A}(\omega) &= -\alpha F_2(\omega) + \alpha F_1(\omega) \int_{-\infty}^{+\infty} \mathrm{d}\omega_1 F_2(\omega_1) Z(\omega - \omega_1) \\ &\quad -(-1)^n \alpha F_1(\omega) \sum_{n=2}^{\infty} \int_{-\infty}^{+\infty} \cdots \int_{-\infty}^{+\infty} \mathrm{d}\omega_1 \cdots \mathrm{d}\omega_n F_1(\omega_1) \cdots F_1(\omega_{n-1}) F_2(\omega_n) Z(\omega - \omega_1) \cdots Z(\omega_{n-1} - \omega_n).\end{aligned}$$

In the regime of weak coupling between the cavity and the system to be measured, we can omit the backaction of the cavity on the measured system. Then $Z(\omega)$ can be written as $Z(\omega) = X(\omega) Z_{\mathrm{in}}(\omega)$, where $X(\omega)$ is the response function of the system, and $Z_{\mathrm{in}}(\omega)$ is the Fourier transform of the input field acting on the system. If we further consider an input field $Z_{\mathrm{in}}(\omega)$ such that $\langle Z_{\mathrm{in}}(\omega) Z_{\mathrm{in}}^*(\omega') \rangle = \delta(\omega - \omega')$, where $\langle \cdot \rangle$ denotes the ensemble average, the cavity spectrum can then be expressed as

$$\tilde{S}(\omega) = |\alpha|^2 S(\omega). \tag{16}$$

The normalized cavity spectrum $S(\omega)$ is given by

$$\begin{aligned}S(\omega) &= G(\omega) S_a(\omega) + G_1(\omega) \int_{-\infty}^{+\infty} \mathrm{d}\omega_1 G_2(\omega_1) S_{zo}(\omega - \omega_1) \\ &\quad + G_1(\omega) \sum_{i=2}^{n} \int_{-\infty}^{+\infty} \cdots \int_{-\infty}^{+\infty} \mathrm{d}\omega_1 \cdots \mathrm{d}\omega_i G_2(\omega_i) G_1(\omega_1) \cdots G_1(\omega_{i-1}) S_{zo}(\omega - \omega_1) \cdots S_{zo}(\omega_{i-1} - \omega_i),\end{aligned} \tag{17}$$

where $G(\omega)$, $G_1(\omega)$, and $G_2(\omega)$ are

$$G(\omega) = \frac{(\gamma^2 + (\omega - \Delta)^2)(\kappa^2 + (\omega - \Delta)^2)}{(\omega - \Delta)^4 + (\omega - \Delta)^2(\kappa^2 + \gamma^2 - 2g_1^2) + (g_1^2 - \gamma\kappa)^2}, \tag{18}$$

$$G_1(\omega) = G(\omega) \frac{g^2}{\kappa^2 + (\omega - \Delta)^2}, \tag{19}$$

$$G_2(\omega) = G(\omega) \frac{2\kappa}{\kappa^2 + (\omega - \Delta)^2}. \tag{20}$$

$S_a(\omega)$ is the background Lorentz spectrum calculated from Eq. (1) by setting the coupling strength $g_1 = 0$ and $S_{zo}(\omega) = |X(\omega)|^2$. Recall that the input of the measured system $Z_{\mathrm{in}}(\omega)$ is a white noise input, thus $S_{zo}(\omega)$ can be seen as the spectrum of the measured system. Moreover, since $G_1(\omega) \propto g^2$, we can ignore the higher-order terms of $G_1(\omega)$ in Eq. (17) in the weak-coupling limit. Then, the normalized cavity spectrum becomes

$$S(\omega) \approx G(\omega) S_a(\omega) + G_1(\omega) \int_{-\infty}^{+\infty} \mathrm{d}\omega_1 G_2(\omega_1) S_{zo}(\omega - \omega_1). \tag{21}$$

If we further assume that the characteristic frequency of the system being measured, denoted by ω_z, is smaller than, or close to, the damping rate κ of the cavity coupled to it, then $G_1(\omega)$ can be approximated in the frequency range from $\omega = \Delta - \omega_z$ to $\omega = \Delta + \omega_z$ as

$$G_1(\omega) \approx G(\omega) \frac{g^2}{\kappa^2}. \tag{22}$$

Substituting this in Eq. (21), we can represent the normalized cavity spectrum as

$$S(\omega) \approx G(\omega) \left[S_a(\omega) + \frac{g^2}{\kappa^2} \int_{-\infty}^{+\infty} \mathrm{d}\omega_1 G_2(\omega_1) S_{zo}(\omega - \omega_1) \right]. \tag{23}$$

A. Background spectrum in the broken-$\mathcal{PT}$ and $\mathcal{PT}$-symmetric regimes

As discussed above, the background spectrum is given by $G(\omega) S_a(\omega)$. We will now study how this background spectrum behaves in the broken- and unbroken- $\mathcal{PT}$-symmetric regimes.

1. Broken-$\mathcal{PT}$ regime

The phase transition takes place at $g_1 = \Gamma$, where $\Gamma = (\kappa + \gamma)/2$. In the regime $g_1 < \Gamma$ (before the phase transition), we have two optical supermodes with the same frequency $\omega = \Delta$ but different damping rates $\Gamma_\pm$. Thus, the background spectrum can be decomposed into two parts

$$G(\omega)S_a(\omega) = \frac{p'}{(\omega-\Delta)^2+\Gamma_-^2} + \frac{p''}{(\omega-\Delta)^2+\Gamma_+^2}, \tag{24}$$

where $p' = \left[(\Gamma_-^2 - \gamma^2)\kappa\right] / \left[(\kappa-\gamma)\sqrt{\Gamma^2 - g_1^2}\right]$, $p'' = \left[(\gamma^2 - \Gamma_+^2)\kappa\right] / \left[(\kappa-\gamma)\sqrt{\Gamma^2 - g_1^2}\right]$, $\Gamma_\pm = \chi \mp \beta'$, $\chi = (\kappa-\gamma)/2$, $\beta = \sqrt{g_1^2 - \Gamma^2} = i\sqrt{\Gamma^2 - g_1^2} = i\beta'$, with $\beta' = \sqrt{\Gamma^2 - g_1^2}$. Note that this decomposition is valid regardless of whether the gain of the active resonator exactly balances or not the loss of the passive resonator.

In the vicinity of the transition point, we have

$$\lim_{g_1\to\Gamma} G(\omega)S_a(\omega) = \frac{2\kappa[(\omega-\Delta)^2+\gamma^2]}{[(\omega-\Delta)^2+\chi^2]^2}. \tag{25}$$

We also find that $G(\omega)$ of Eq. (18) becomes

$$\lim_{g_1\to\Gamma} G(\omega) = \frac{[\gamma^2+(\omega-\Delta)^2][\kappa^2+(\omega-\Delta)^2]}{[(\omega-\Delta)^2+\chi^2]^2} = \frac{\kappa^2+(\omega-\Delta)^2}{2\kappa}\lim_{g_1\to\Gamma} G(\omega)S_a(\omega). \tag{26}$$

Since $\lim_{g_1\to\Gamma} G(\omega)S_a(\omega) = [\lim_{g_1\to\Gamma} G(\omega)]\,[\lim_{g_1\to\Gamma} S_a(\omega)]$, we arrive at

$$\lim_{g_1\to\Gamma} S_a(\omega) = \frac{2\kappa}{\kappa^2+(\omega-\Delta)^2}. \tag{27}$$

Moreover, if the gain and loss are exactly balanced (i.e., $\kappa = \gamma$), we have $\chi = 0$ and $\Gamma = \kappa = \gamma$, which leads to

$$\lim_{\kappa\to\gamma}\lim_{g_1\to\Gamma} G(\omega)S_a(\omega) = \frac{2\gamma[(\omega-\Delta)^2+\gamma^2]}{(\omega-\Delta)^4} = \frac{2\kappa[(\omega-\Delta)^2+\kappa^2]}{(\omega-\Delta)^4}. \tag{28}$$

Finally, in the limit with very weak coupling such that $g_1 \to 0$, we find that $G(\omega)$ in Eq. (18) goes to one, that is $\lim_{g_1\to 0} G(\omega) = 1$. Moreover, the background spectrum given in Eq. (24) becomes

$$\lim_{g_1\to 0} G(\omega)S_a(\omega) = \lim_{g_1\to 0} S_a(\omega) = \lim_{g_1\to 0} G_2(\omega) = \frac{2\kappa}{(\omega-\Delta)^2+\kappa^2}, \tag{29}$$

and we find

$$\lim_{g_1\to 0} S_a(\omega) = \frac{2\kappa}{(\omega-\Delta)^2+\kappa^2}. \tag{30}$$

2. $\mathcal{PT}$-symmetric regime

This regime is identified with $g_1 > \Gamma$, where there are two resonant peaks with different frequencies, namely at $\omega = \Omega_-$ and $\omega = \Omega_+$, but the same damping rates $\Gamma_\pm = \chi$ [see Fig 1(b)]. The background spectrum can be decomposed into three parts:

$$G(\omega)S_a(\omega) = \frac{2\kappa}{(\omega-\Omega_-)^2+\Gamma_\pm^2} + \frac{\kappa}{(\omega-\Omega_+)^2+\Gamma_\pm^2} + \frac{2\kappa(\kappa\gamma+\gamma^2-g_1^2)}{[(\omega-\Omega_+)^2+\Gamma_\pm^2][(\omega-\Omega_-)^2+\Gamma_\pm^2]}, \tag{31}$$

where $\Omega_\pm = \Delta \pm \beta$ and β is a real number. Note that $G(\omega)S_a(\omega)$ can also be re-written as

$$G(\omega)S_a(\omega) = \frac{2[(\omega-\Delta)^2+\gamma^2]}{[(\omega-\Delta)^2-\beta^2]^2 + 2\chi^2\left[(\omega-\Delta)^2+\beta^2\right]+\chi^4} \tag{32}$$

$$= \frac{2[(\omega-\Delta)^2+\gamma^2]}{[(\omega-\Delta)^2-g_1^2+\Gamma^2]^2 + 2\chi^2\left[(\omega-\Delta)^2+g_1^2-\Gamma^2\right]+\chi^4} \tag{33}$$

In the vicinity of the transition point, we find from Eq. (33) that

$$\lim_{g_1\to\Gamma} G(\omega)S_a(\omega) = \frac{2\kappa[(\omega-\Delta)^2+\gamma^2]}{[(\omega-\Delta)^2+\chi^2]^2}. \tag{34}$$

Note that the $\lim_{g_1\to\Gamma} G(\omega)$ given in Eq. (26) is the same for both the $\mathcal{PT}$-symmetric regime and the broken-$\mathcal{PT}$ regime. Substituting Eq. (26) in Eq. (34), we find

$$\lim_{g_1\to\Gamma} S_a(\omega) = \frac{2\kappa}{\kappa^2+(\omega-\Delta)^2}, \tag{35}$$

which is the same as the case for the broken-$\mathcal{PT}$ case.

Moreover, if the gain and loss are exactly balanced (i.e., $\kappa=\gamma$), we have $\Gamma=\kappa=\gamma$ and $\chi=0$ (i.e., implying supermodes with zero linewidth). Then we obtain

$$\lim_{\kappa\to\gamma}\lim_{g_1\to\Gamma} G(\omega)S_a(\omega) = \frac{2\kappa[(\omega-\Delta)^2+\kappa^2]}{(\omega-\Delta)^4} = \frac{2\gamma[(\omega-\Delta)^2+\gamma^2]}{(\omega-\Delta)^4}, \tag{36}$$

which is exactly the same as Eq. (29), implying that the background spectrum converges to the same spectrum in the vicinity of the $\mathcal{PT}$-phase transition point.

Finally, in the very-*strong*-coupling limit, that is in the limit when $g_1\to\infty$, we find that the $G(\omega)$ in Eq. (18) goes to zero, that is $\lim_{g_1\to\infty} G(\omega)=0$, and hence the background spectrum given in Eq. (31) satifies:

$$\lim_{g_1\to\infty} G(\omega)S_a(\omega) = \lim_{g_1\to\infty} G_1(\omega) = \lim_{g_1\to\infty} G_2(\omega) = 0. \tag{37}$$

B. Sideband spectrum in the broken-$\mathcal{PT}$ and $\mathcal{PT}$-symmetric regimes

The sideband spectrum corresponds to the second term $(g^2/\kappa^2)G(\omega)\int_{-\infty}^{+\infty} G_2(\omega_1)S_{zo}(\omega-\omega_1)\mathrm{d}\omega_1$ in Eq. (23). The integral term in Eq. (23) is a convolution in the frequency domain, and can be reexpressed in the time domain by introducing the Fourier transform $\mathcal{F}$ as a product of $G_2(t)$ and $S_{zo}(t)$

$$\int_{-\infty}^{+\infty} \mathrm{d}\omega_1 G_2(\omega_1)S_{zo}(\omega-\omega_1) = \mathcal{F}[G_2(t)S_{zo}(t)], \tag{38}$$

where $G_2(t)$ and $S_{zo}(t)$ are the inverse Fourier transforms of $G_2(\omega)$ and $S_{zo}(\omega)$.

1. *Broken-$\mathcal{PT}$ regime*

In the regime defined by $g_1<\Gamma$, $G_2(\omega)$ can be decomposed into two parts as

$$G_2(\omega) = p_-\frac{\Gamma_-^2}{(\omega-\Delta)^2+\Gamma_-^2} + p_+\frac{\Gamma_+^2}{(\omega-\Delta)^2+\Gamma_+^2}, \tag{39}$$

where $p_- = \left[(\Gamma_-^2-\gamma^2)\kappa\right] / \left[(\kappa-\gamma)\Gamma_-^2\sqrt{\Gamma^2-g_1^2}\right]$, $p_+ = \left[(\gamma^2-\Gamma_+^2)\kappa\right] / \left[(\kappa-\gamma)\Gamma_+^2\sqrt{\Gamma^2-g_1^2}\right]$, $\Gamma=(\kappa+\gamma)/2$, $\Gamma_\pm = \chi\mp\sqrt{\Gamma^2-g_1^2}$, and $\chi=(\kappa-\gamma)/2$. The inverse Fourier transform of $G_2(\omega)$ can be expressed as

$$G_2(t) = c_1\exp(-\Gamma_-|t|+i\Delta t) + d_1\exp(-\Gamma_+|t|+i\Delta t), \tag{40}$$

where

$$c_1 = \frac{\Gamma_-^2-\gamma^2}{2(\kappa-\gamma)\sqrt{\Gamma^2-g_1^2}}\frac{\kappa}{\Gamma_-}, \tag{41}$$

$$d_1 = \frac{\gamma^2-\Gamma_+^2}{2(\kappa-\gamma)\sqrt{\Gamma^2-g_1^2}}\frac{\kappa}{\Gamma_+}. \tag{42}$$

Substituting these equations in Eq. (38), we find

$$\int_{-\infty}^{+\infty} \mathrm{d}\omega_1 G_2(\omega_1) S_{zo}(\omega-\omega_1) = c_1 S_{z1}(\omega) + d_1 S_{z2}(\omega), \tag{43}$$

where $S_{z1}(\omega) = \mathcal{F}\left[f_1(t)\mathcal{F}^{-1}[S_{zo}(\omega)]\right]$, $S_{z2}(\omega) = \mathcal{F}\left[f_2(t)\mathcal{F}^{-1}[S_{zo}(\omega)]\right]$, and $\mathcal{F}^{-1}$ is the inverse Fourier transform. Here, $f_1(t)$ and $f_2(t)$ are form factors, which can be represented by $f_1(t) = \exp(-\Gamma_-|t| + i\Delta t)$ and $f_2(t) = \exp(-\Gamma_+|t| + i\Delta t)$.

In the vicinity of the phase-transition point ($g_1 \to \Gamma$), we have

$$\lim_{g_1\to\Gamma}(c_1 S_{z1}(\omega) + d_1 S_{z2}(\omega)) = \lim_{g_1\to\Gamma}(c_1+d_1)\mathcal{F}\left[f(t)\mathcal{F}^{-1}[S_{zo}(\omega)]\right],$$

where $f(t) = \exp\left\{-[(\kappa-\gamma)/2]|t| + i\Delta t\right\}$ is obtained as $\lim_{g_1\to\Gamma} f_1(t) = \lim_{g_1\to\Gamma} f_2(t) = f(t)$. Then, explicitly writing the expressions Γ_- and Γ_+ in c_1 [Eq. (41)] and d_1 [Eq. (42)], we can find that

$$\lim_{g_1\to\Gamma}(c_1+d_1) = \frac{\kappa}{\kappa-\gamma}\frac{\chi^2+\gamma^2}{\chi^2} = \frac{\kappa}{\kappa-\gamma}\left(1+(\gamma/\chi)^2\right) = \frac{\kappa}{\kappa-\gamma}\left[1+\frac{4\gamma^2}{(\kappa-\gamma)^2}\right]. \tag{44}$$

Subsequently, we have

$$\lim_{g_1\to\Gamma}\int_{-\infty}^{+\infty} \mathrm{d}\omega_1 G_2(\omega_1) S_{zo}(\omega-\omega_1) = \frac{\kappa}{\kappa-\gamma}\left[1+\frac{4\gamma^2}{(\kappa-\gamma)^2}\right]\mathcal{F}\left[f(t)\mathcal{F}^{-1}[S_{zo}(\omega)]\right]. \tag{45}$$

Away from the phase-transition point, Γ_- is much larger than Γ_+, which means that d_1 is much larger than c_1. If we now assume that $S_{zo}(\omega)$ has a Lorentzian form, we find that $S_{z2}(\omega)$ is much narrower than $S_{z1}(\omega)$, implying that the sideband $d_1 S_{z2}(\omega)$ in $S(\omega)$ induced by the back-action spectrum $S_{zo}(\omega)$ is higher and narrower than the other sideband $c_1 S_{z1}(\omega)$ in $S(\omega)$ also induced by the back-action spectrum $S_{zo}(\omega)$. Thus, $c_1 S_{z1}(\omega)$ can be ignored. Consequently, we can re-write Eq. (43) as

$$\int_{-\infty}^{+\infty} \mathrm{d}\omega_1 G_2(\omega_1) S_{zo}(\omega-\omega_1) = d_1 S_{z2}(\omega) = \frac{\kappa}{(\kappa-\gamma)}\frac{\gamma^2-\Gamma_+^2}{\sqrt{\Gamma^2-g_1^2\Gamma_+}} S_{z2}(\omega). \tag{46}$$

In the very *weak* coupling limit, that is in the limit when $g_1 \to 0$, we find that c_1 of Eq. (41) goes to 1 whereas d_1 of Eq. (42) goes to zero. The form factor $f_1(t)$ then becomes $f(t) = \lim_{g_1\to 0} f_1(t) = \exp(-\kappa|t| + i\Delta t)$. Subsequently, we can rewrite Eq. (43) as

$$\lim_{g_1\to 0}\int_{-\infty}^{+\infty} \mathrm{d}\omega_1 G_2(\omega_1) S_{zo}(\omega-\omega_1) = S_{z3}(\omega), \tag{47}$$

where $S_{z3}(\omega) = \mathcal{F}\left[f(t)\mathcal{F}^{-1}[S_{zo}(\omega)]\right]$.

2. $\mathcal{PT}$-symmetric regime

In this regime, where we have $g_1 > \Gamma$, $G_2(\omega)$ can be decomposed into three parts as

$$G_2(\omega) = p_1\frac{\Gamma_\pm^2}{(\omega-\Omega_-)^2+\Gamma_\pm^2} + p_2\frac{\Gamma_\pm^2}{(\omega-\Omega_+)^2+\Gamma_\pm^2} + p_3\frac{\Gamma_\pm^4}{\left[(\omega-\Omega_+)^2+\Gamma_\pm^2\right]\left[(\omega-\Omega_-)^2+\Gamma_\pm^2\right]}, \tag{48}$$

where $p_1 = 2\kappa/\Gamma_\pm^2$, $p_2 = 2\kappa/\Gamma_\pm^2$, $p_3 = 2\kappa(\kappa\gamma+\gamma^2-g_1^2)/\Gamma_\pm^4$, $\Omega_\pm = \Delta \pm \sqrt{g_1^2-\Gamma^2}$, and $\Gamma_\pm = \chi$. The first two terms on the right side of Eq. (48) can be easily transformed into the time domain by inverse Fourier transforms yielding:

$$\mathcal{F}^{-1}\left[p_1\frac{\Gamma_\pm^2}{(\omega-\Omega_-)^2+\Gamma_\pm^2}\right] = \frac{\kappa}{\Gamma_\pm}\exp(-\Gamma_\pm|t| + i\Omega_- t), \tag{49}$$

and

$$\mathcal{F}^{-1}\left[p_2\frac{\Gamma_\pm^2}{(\omega-\Omega_+)^2+\Gamma_\pm^2}\right] = \frac{\kappa}{\Gamma_\pm}\exp(-\Gamma_\pm|t| + i\Omega_+ t). \tag{50}$$

The third term is a convolution term in time domain which can be represented by

$$\mathcal{F}^{-1}\left[p_3\frac{\Gamma_\pm^4}{\left[(\omega-\Omega_+)^2+\Gamma_\pm^2\right]\left[(\omega-\Omega_-)^2+\Gamma_\pm^2\right]}\right]=\frac{\kappa(\kappa\gamma+\gamma^2-g_1^2)}{\Gamma_\pm^2}\int_{-\infty}^{+\infty}\mathrm{d}\tau f_3(\tau)f_4(t-\tau), \tag{51}$$

where $f_3(t)=\exp(-\Gamma_\pm|t|-i\Omega_+t)$ and $f_4(t)=\exp(-\Gamma_\pm|t|-i\Omega_-t)$. The integral term in Eq. (51) equals to

$$\begin{aligned}\int_{-\infty}^{+\infty}f_3(\tau)f_4(t-\tau)\mathrm{d}\tau=&\frac{\Gamma_\pm}{(g_1^2-\kappa\gamma)}\left[\exp\left(-\Gamma_\pm|t|+i\Omega_+t\right)+\exp\left(-\Gamma_\pm|t|+i\Omega_-t\right)\right]\\&+\frac{1}{\sqrt{g_1^2-\Gamma^2}}\frac{\Gamma_\pm^2}{g_1^2-\kappa\gamma}\left[i\mathrm{sgn}(t)\exp(-\Gamma_\pm|t|+i\Omega_+t)+i\mathrm{sgn}(t)\exp(-\Gamma_\pm|t|+i\Omega_-t)\right],\end{aligned} \tag{52}$$

where $\mathrm{sgn}(t)$ is the sign function defined by

$$\mathrm{sgn}(t)=\begin{cases}1, & t>0\\ 0, & t=0.\\ -1, & t<0\end{cases} \tag{53}$$

Using Eqs. (49)-(52), we can write the time domain expression $G_2(t)$ for $G_2(\omega)$ as

$$\begin{aligned}G_2(t)=\mathcal{F}^{-1}[G_2(\omega)]=&\left[\frac{\kappa}{\Gamma_\pm}+\frac{\kappa(\kappa\gamma+\gamma^2-g_1^2)}{\Gamma_\pm(g_1^2-\kappa\gamma)}\right]\left[\exp\left(-\Gamma_\pm|t|+i\Omega_+t\right)+\exp\left(-\Gamma_\pm|t|+i\Omega_-t\right)\right]\\&+\frac{1}{\sqrt{g_1^2-\Gamma^2}}\frac{\kappa(\kappa\gamma+\gamma^2-g_1^2)}{g_1^2-\kappa\gamma}\left[i\mathrm{sgn}(t)\exp(-\Gamma_\pm|t|+i\Omega_+t)+i\mathrm{sgn}(t)\exp(-\Gamma_\pm|t|+i\Omega_-t)\right].\end{aligned} \tag{54}$$

Substituting Eq. (54) into Eq. (38), we find

$$\int_{-\infty}^{+\infty}\mathrm{d}\omega_1 G_2(\omega_1)S_{zo}(\omega-\omega_1)=\frac{\kappa\gamma^2}{\Gamma_\pm(g_1^2-\kappa\gamma)}S_{z4}(\omega)+\frac{1}{\sqrt{g_1^2-\Gamma^2}}\frac{\kappa(\kappa\gamma+\gamma^2-g_1^2)}{g_1^2-\kappa\gamma}S_{z5}(\omega), \tag{55}$$

where $S_{z4}(\omega)=\mathcal{F}\left[f_5(t)\mathcal{F}^{-1}[S_{zo}(\omega)]\right]$, with $f_5(t)=\exp(-\Gamma_\pm|t|+i\Omega_+t)+\exp(-\Gamma_\pm|t|+i\Omega_-t)$, and $S_{z5}(\omega)=\mathcal{F}\left[f_6(t)\mathcal{F}^{-1}[S_{zo}(\omega)]\right]$, with $f_6(t)=i\mathrm{sgn}(t)\exp(-\Gamma_\pm|t|+i\Omega_+t)+i\mathrm{sgn}(t)\exp(-\Gamma_\pm|t|+i\Omega_-t)$.

In the vicinity of the phase-transition point ($g_1\to\Gamma$), we can omit the high-order terms of $(g_1^2-\Gamma^2)$ in $S_{z5}(\omega)$. Also note that in the $\mathcal{PT}$-symmetric regime, we have $\Gamma_\pm=\chi=(\kappa-\gamma)/2$. Substituting these expressions into Eq. (55), we have

$$\lim_{g_1\to\Gamma}\int_{-\infty}^{+\infty}\mathrm{d}\omega_1 G_2(\omega_1)S_{zo}(\omega-\omega_1)=\frac{\kappa\gamma^2}{\chi(\Gamma^2-\kappa\gamma)}S_{z6}(\omega)=\frac{2}{\kappa-\gamma}\frac{\kappa\gamma^2}{\Gamma^2-\kappa\gamma}S_{z6}(\omega)=\frac{8\kappa\gamma^2}{(\kappa-\gamma)^3}S_{z6}(\omega) \tag{56}$$

where we have used $\Gamma=(\kappa+\gamma)/2$, and $S_{z6}(\omega)=\mathcal{F}\left[f(t)\mathcal{F}^{-1}[S_{zo}(\omega)]\right]$, with $f(t)=\exp(-\Gamma_\pm|t|-i\Omega t)$.

In the $\mathcal{PT}$-symmetric regime, but far away from the phase-transition point, we can assume that S_{zo} is in the Lorentzian form $r_z/[(\omega-\omega_z)^2+r_z^2]$, where r_z and ω_z are, respectively, the decay rate and the frequency of the system being measured. Then $S_{z4}(\omega)$ and $S_{z5}(\omega)$ can be expressed as

$$S_{z4}(\omega) = \frac{r_z+\Gamma_\pm}{(\omega-\omega_z-\Omega_+)^2+(r_z+\Gamma_\pm)^2}+\frac{r_z+\Gamma_\pm}{(\omega-\omega_z-\Omega_-)^2+(r_z+\Gamma_\pm)^2}, \tag{57}$$

$$S_{z5}(\omega) = \frac{\omega-\omega_z-\Omega_+}{(\omega-\omega_z-\Omega_+)^2+(r_z+\Gamma_\pm)^2}+\frac{\omega-\omega_z-\Omega_-}{(\omega-\omega_z-\Omega_-)^2+(r_z+\Gamma_\pm)^2}. \tag{58}$$

Note that $S_{z4}(\omega)$ has two peaks centered at the frequencies $(\Omega_++\omega_z)$ and $(\Omega_-+\omega_z)$. Similarly, $S_{z5}(\omega)$, too, has two peaks with central frequencies at $\Omega_++\omega_z+r_z+\Gamma_\pm$ and $\Omega_-+\omega_z+r_z+\Gamma_\pm$. If $r_z\ll\omega_z$ and $\Gamma_\pm=\chi=(\kappa-\gamma)/2\approx r_z$, the four peaks in $S(\omega)$ induced by $S_{z4}(\omega)$ and $S_{z5}(\omega)$ are merged into two peaks at the frequencies $(\Omega_++\omega_z)$ and $(\Omega_-+\omega_z)$. Since in the $\mathcal{PT}$-symmetric regime, the background spectrum also has two peaks at the frequencies Ω_+ and Ω_-, we can focus on the frequency domain ranging from Ω_+ to $\Omega_++\omega_z$. Under this condition, $S_{z5}(\omega)$ can be ignored, and Eq. (55) can be written as

$$\int_{-\infty}^{+\infty}\mathrm{d}\omega_1 G_2(\omega_1)S_{zo}(\omega-\omega_1)=\frac{\kappa\gamma^2}{\Gamma_\pm(g_1^2-\kappa\gamma)}S_{z4}(\omega)=\frac{\kappa\gamma^2}{\chi(\Gamma^2-\kappa\gamma)}S_{z4}(\omega)=\frac{2}{\kappa-\gamma}\frac{\kappa\gamma^2}{g_1^2-\kappa\gamma}S_{z4}(\omega). \tag{59}$$

In the very strong coupling limit, that is in the limit when $g_1 \to \infty$, we find that $G(\omega)$ in Eq. (18) goes to zero, that is $\lim_{g_1\to\infty} G(\omega) = 0$ and hence the background spectrum given in Eq. (31), too:

$$\lim_{g_1\to\infty} G(\omega)S_a(\omega) = \lim_{g_1\to\infty} G_1(\omega) = \lim_{g_1\to\infty} G_2(\omega) = 0. \tag{60}$$

C. Normalized cavity spectrum in the broken-$\mathcal{PT}$ and $\mathcal{PT}$-symmetric regimes

In the previous subsections, we have derived the background and sideband spectra and presented the expressions for the regimes before and after the phase transition point. Here, we combine those expressions to present the results for the overall spectrum given in Eq. (23):

$$S(\omega) \approx G(\omega)\left[S_a(\omega) + \frac{g^2}{\kappa^2}\int_{-\infty}^{+\infty} G_2(\omega_1)S_{zo}(\omega-\omega_1)\mathrm{d}\omega_1\right]. \tag{61}$$

Here, we will focus on the spectra in the vicinity of the transition point.

1. *Broken-$\mathcal{PT}$ regime*

Substituting into Eq. (61) the expressions for the background spectrum given in Eq. (24) and the sideband spectrum given into Eq. (43), we find the $S(\omega)$ as

$$S(\omega) = G(\omega)\left[S_a(\omega) + \frac{g^2}{\kappa^2}c_1 S_{z1}(\omega) + \frac{g^2}{\kappa^2}d_1 S_{z2}(\omega)\right]. \tag{62}$$

In the vicinity of the transition point ($g_1 \to \Gamma$), using the expressions in Eqs. (25) and (45), we can express the normalized cavity spectrum as

$$\lim_{g_1\to\Gamma} S(\omega) = G(\omega)\left[S_a(\omega) + AS_z(\omega)\right], \tag{63}$$

where we have defined

$$A = \frac{g^2}{\kappa^2}\frac{\kappa}{\kappa-\gamma}\left[1 + \frac{4\gamma^2}{(\kappa-\gamma)^2}\right] \tag{64}$$

as the amplification factor, and $S_z(\omega) = \mathcal{F}\left[f(t)\mathcal{F}^{-1}[S_{zo}(\omega)]\right]$ with $f(t) = \exp\{-[(\kappa-\gamma)/2]|t| + i\Delta t\} = \exp(-\chi|t| + i\Delta t)$, as defined previously. If $\kappa \to \gamma$ (i.e., exact balance between gain and loss), the amplification factor $A \to \infty$, implying that in the vicinity of the transition point with well-balanced loss and gain, the amplification factor can be very high.

In this regime, but away from the phase-transition point, we have

$$S(\omega) = G(\omega)\left[S_a(\omega) + A(g, g_1)S_{z4}(\omega)\right]. \tag{65}$$

Using Eq. (64) in Eq. (46), we find that the amplification factor $A(g, g_1)$ can be written as

$$A(g, g_1) = \frac{g^2(\gamma^2 - \Gamma_+^2)}{2\kappa(\kappa-\gamma)\sqrt{\Gamma^2 - g_1^2}\Gamma_+}. \tag{66}$$

Finally, in the very weak coupling limit $g_1 \to 0$, using Eqs. (29) and (47), we find the normalized spectrum as

$$S(\omega) \approx S_a(\omega) + \frac{g^2}{\kappa^2}S_{z3}(\omega), \tag{67}$$

where $S_{z3}(\omega) = \mathcal{F}\left[f(t)\mathcal{F}^{-1}[S_{zo}(\omega)]\right]$, $f(t) = \exp(-\kappa|t| + i\Delta t)$, and the amplification factor is given by $A = g^2/\kappa^2$.

2. $\mathcal{PT}$-symmetric regime

Substituting Eq. (31) and Eq. (55) into Eq. (61), we can express the normalized cavity spectrum as

$$S(\omega) = G(\omega)\left[S_a(\omega) + \frac{g^2}{\kappa^2}\frac{\kappa\gamma^2}{\Gamma_\pm(g_1^2-\kappa\gamma)}S_{z4}(\omega) + \frac{g^2}{\kappa^2}\frac{1}{\sqrt{g_1^2-\Gamma^2}}\frac{\kappa(\kappa\gamma+\gamma^2-g_1^2)}{g_1^2-\kappa\gamma}S_{z5}(\omega)\right], \tag{68}$$

where $S_{z4}(\omega) = \mathcal{F}\left[f_5(t)\mathcal{F}^{-1}[S_{zo}(\omega)]\right]$, with $f_5(t) = \exp(-\Gamma_\pm|t| + i\Omega_+ t) + \exp(-\Gamma_\pm|t| + i\Omega_- t)$, and $S_{z5}(\omega) = \mathcal{F}\left[f_6(t)\mathcal{F}^{-1}[S_{zo}(\omega)]\right]$, with $f_6(t) = i\mathrm{sgn}(t)\exp(-\Gamma_\pm|t| - i\Omega_+ t) + i\mathrm{sgn}(t)\exp(-\Gamma_\pm|t| - i\Omega_- t)$.

In the vicinity of the phase-transition point $g_1 \to \Gamma$, we use Eqs. (34) and (56) to arrive at

$$\lim_{g_1\to\Gamma} S(\omega) = G(\omega)\left[S_a(\omega) + \frac{g^2}{\kappa^2}\frac{8\kappa^3}{(\kappa-\gamma)^3}S_{z6}(\omega)\right] = G(\omega)\left[S_a(\omega) + \frac{8g^2\kappa}{(\kappa-\gamma)^3}S_{z6}(\omega)\right]. \tag{69}$$

Then the amplification factor is given by

$$A(g) = \frac{8g^2\kappa}{(\kappa-\gamma)^3}, \tag{70}$$

which approaches infinity as κ approaches γ, implying that the closer the gain to the loss, the higher the amplification.

In the $\mathcal{PT}$-symmetric regime, but far away from the phase-transition point, the normalized cavity spectrum can be recasted as

$$S(\omega) = G(\omega)\left[S_a(\omega) + \frac{g^2}{\kappa^2}\frac{2}{\kappa-\gamma}\frac{\kappa\gamma^2}{g_1^2-\kappa\gamma}S_{z4}(\omega)\right]. \tag{71}$$

Then the amplification factor is given by

$$A(g, g_1) = \frac{g^2}{\kappa^2}\frac{2}{\kappa-\gamma}\frac{\kappa\gamma^2}{g_1^2-\kappa\gamma} = \frac{2g^2\gamma^2}{\kappa(\kappa-\gamma)}\frac{1}{g_1^2-\kappa\gamma}. \tag{72}$$

Clearly, $A(g, g_1)$ can be made very high by having $\kappa\gamma$ closer to g_1, or by increasing the coupling strength g of the optical modes.

Finally, in the very strong coupling limit $g_1 \to \infty$, we find, using Eqs. (37) and (60), that

$$S(\omega) = 0. \tag{73}$$

and thus there is no amplification.

In Figs. 1a and 1b, we present the amplification factor $A(g_1, g)$ as a function of the normalized coupling strength g_1/Γ for two different gain-to-loss ratios γ/κ. It is clearly seen that in the vicinity of the phase transition point, $A(g_1, g)$ takes its maximum value, and it reaches higher values as γ/κ approaches one. An increase from $\gamma/\kappa = 0.8$ to $\gamma/\kappa = 0.999$ leads to a remarkable 100-fold increase: from $A(g_1, g) = 10$ to $A(g_1, g) = 1000$. Moreover, as we approach to (or move away from) the transition point, the change in $A(g_1, g)$ is sharper in the broken-$\mathcal{PT}$ regime than in the $\mathcal{PT}$-symmetric regime. Therefore, in the regions away from the phase transition point, $A(g_1, g)$ has higher values in the $\mathcal{PT}$-symmetric regime than in the broken-$\mathcal{PT}$ regime.

Figures 1c and 1d depict the normalized background spectra $S_a(\omega)$ of the two-cavity system (i.e., one cavity with gain and the other with loss) in the broken- and unbroken-$\mathcal{PT}$-symmetric regimes, in comparison with the spectra of a single-cavity system for two different gain-to-loss ratios γ/κ. As expected in the $\mathcal{PT}$-symmetric regime, the spectra show mode splitting which is characterized by the presence of the two resonant dips. In the broken-$\mathcal{PT}$-symmetric regime, the modes coalesce and there is only one resonant dip. Compared to the single-cavity system composed of only one passive (with loss) resonator, the resonant dips for the two-cavity system are narrower due to the presence of the gain. As the gain-to-loss ratio increases, the spectra become much narrower.

II. AMPLIFICATION IN A SYSTEM WITH TWO COUPLED LOSSY CAVITIES

A. Zero-frequency detuning

In order to understand the effect of gain in our $\mathcal{PT}$-symmetric system, we consider here a coupled-cavity system composed of two lossy cavities (i.e., we replace the active cavity with a passive lossy cavity). The non-Hermitian Hamiltonian of this system is described as

$$H = (\Delta - i\kappa)\, a^\dagger a + (\Delta - i\kappa_1)\, c^\dagger c + g_1(a^\dagger c + c^\dagger a) + g a^\dagger a z, \tag{74}$$

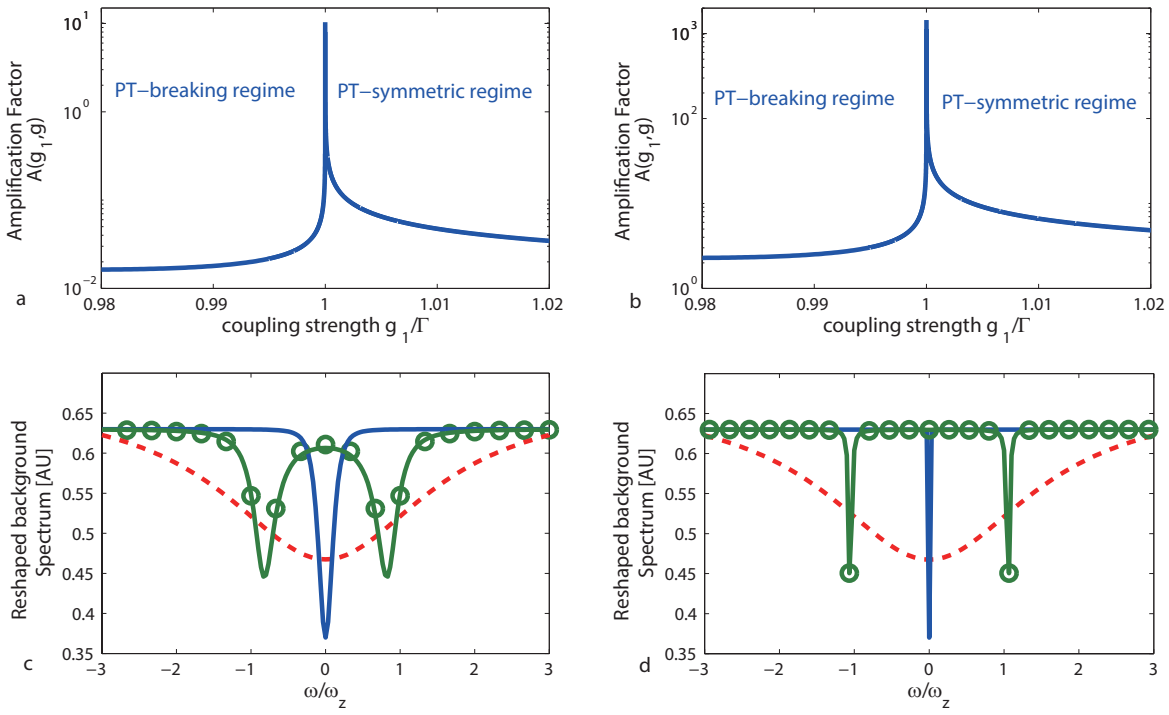

FIG. 1: (Color online) (a,b) Amplification factor $A(g_1, g)$ of the backaction spectrum versus the normalized coupling strength g_1/Γ between the cavity and the system being measured with $\omega_z = 3$MHz and $\kappa = 10$MHz, when (a) $\gamma = 8$MHz (i.e., gain-to-loss ratio $\gamma/\kappa = 0.8$) and (b) $\gamma = 9.99$MHz (i.e., gain-to-loss ratio $\gamma/\kappa = 0.999$). Note that there is a remarkable 100-fold increase in the maximum value of $A(g_1, g)$ when γ/κ is increased from its value of 0.8 in (a) to 0.999 in (b). (c,d) Normalized background spectrum $S_a(\omega)$ of a single-cavity system (red dashed curve), and of the two-cavity system (one with loss and the other with gain) in the broken-$\mathcal{PT}$ regime (blue curve) and in the $\mathcal{PT}$-symmetric regime (green curve with circular marks) at $\omega_z = 3$MHz and $\kappa = 10$MHz when (c) $\gamma = 8$MHz (i.e., $\gamma/\kappa = 0.8$) and (d) $\gamma = 9.99$MHz (i.e., $\gamma/\kappa = 0.999$). In the $\mathcal{PT}$-symmetric regime, the spectrum shows splitting (two resonant dips) whereas in the broken-$\mathcal{PT}$ regime there is no mode splitting (single resonant dip). Note that due to the presence of the gain in the two-cavity system, the spectra (resonant dips) in the broken- and unbroken-$\mathcal{PT}$-symmetric regime are much narrower than those for the single-cavity case.

which differs from the Hamiltonian of the passive-active cavity system given in Eq. (1) in the second term which is now $(\Delta - i\kappa_1)\, c^\dagger c$ instead of $(\Delta + i\gamma)\, c^\dagger c$ in Eq. (1). In other words, we replace γ with $-\kappa_1$ to accommodate the passive lossy resonator, and κ_1 now denotes the damping rate of the cavity with the optical mode c. The rest of the parameters are defined in the same way as before. To make a distinction with the active-passive system, in the following discussion we will denote the variables and functions for the passive-passive system with a "tilde" over them, e.g., $\tilde{f}$.

By replacing γ with $-\kappa_1$, we find that $\tilde{\chi} = (\kappa + \kappa_1)/2$, $\tilde{\Gamma} = (\kappa - \kappa_1)/2$, and $\tilde{\beta} = \sqrt{g_1^2 - \tilde{\Gamma}^2}$. Consequently, using Eq. (3) we find that the effective coupling strength $\tilde{g}_{\rm eff}$ for the passive-passive system can be written as

$$\tilde{g}_{\rm eff} = \frac{g\left(\tilde{\Gamma} + \sqrt{\tilde{\Gamma}^2 - g_1^2}\right)}{2\sqrt{\tilde{\Gamma}^2 - g_1^2}}. \tag{75}$$

One can easily show that $\tilde{g}_{\rm eff}$ cannot be larger than $g_{\rm eff}$.

From the expression $\tilde{\beta} = \sqrt{g_1^2 - \tilde{\Gamma}^2}$, it is clear that there is a phase transition at the point $g_1 = \tilde{\Gamma}$. This point is called an exceptional point (EP). Similar to the case of active-passive resonators, the coupled passive-passive system has two optical supermodes with complex frequencies $\tilde{\omega}_\pm$, whose real and imaginary parts are given as $\tilde{\Omega}_\pm$ and $\tilde{\Gamma}_\pm$, respectively. When $\tilde{\Gamma} = (\kappa - \kappa_1)/2 < g_1$, the two supermodes are nondegenerate with different real parts (resonance frequencies) $\tilde{\Omega}_\pm = \Delta \pm \sqrt{g_1^2 - \tilde{\Gamma}^2}$ and the same imaginary parts (damping rates) $\tilde{\Gamma}_\pm = (\kappa + \kappa_1)/2$. On the other hand, when $\tilde{\Gamma} = (\kappa - \kappa_1)/2 > g_1$, the two supermodes are degenerate with the same resonant frequencies $\tilde{\Omega}_\pm = \Delta$,

but different damping rates $\tilde{\Gamma}_{\pm}=(\kappa+\kappa_1)/2\mp\sqrt{\tilde{\Gamma}^2-g_1^2}$. We will refer to the regime for $\tilde{\Gamma}=(\kappa-\kappa_1)/2<g_1$ as the regime after the EP, and the regime for $\tilde{\Gamma}=(\kappa-\kappa_1)/2>g_1$ as the regime before the EP.

Following the same line of reasoning as the $\mathcal{PT}$-case (active-passive system), we can write the normalized spectrum of the cavity as

$$\begin{aligned}\tilde{S}(\omega) &= \tilde{G}(\omega)S_a(\omega)+\tilde{G}_1(\omega)\int_{-\infty}^{+\infty}\mathrm{d}\omega_1\tilde{G}_2(\omega_1)S_{zo}(\omega-\omega_1)\\ &+\tilde{G}_1(\omega)\sum_{i=2}^{n}\int_{-\infty}^{+\infty}\cdots\int_{-\infty}^{+\infty}\mathrm{d}\omega_1\cdots\mathrm{d}\omega_i\tilde{G}_2(\omega_i)\tilde{G}_1(\omega_1)\cdots\tilde{G}_1(\omega_{i-1})S_{zo}(\omega-\omega_1)\cdots S_{zo}(\omega_{i-1}-\omega_i),\end{aligned}\tag{76}$$

where

$$\begin{aligned}\tilde{G}(\omega) &= \frac{(\kappa_1^2+(\omega-\Delta)^2)(\kappa^2+(\omega-\Delta)^2)}{(\omega-\Delta)^4+(\omega-\Delta)^2(\kappa^2+\kappa_1^2-2g_1^2)+(g_1^2+\kappa_1\kappa)^2},\\ \tilde{G}_1(\omega) &= \tilde{G}(\omega)\frac{g^2}{\kappa^2+(\omega-\Delta)^2},\\ \tilde{G}_2(\omega) &= \tilde{G}(\omega)\frac{\kappa}{\kappa^2+(\omega-\Delta)^2}.\end{aligned}$$

$S_a(\omega)$ and $S_{zo}(\omega)$ are defined with the same meanings of those in our $\mathcal{PT}$-symmetric metrology system. The spectrum of the cavity in this case can be re-expressed as

$$\tilde{S}(\omega)\approx\tilde{G}(\omega)S_a(\omega)+\tilde{G}_1(\omega)\int_{-\infty}^{+\infty}\mathrm{d}\omega_1\tilde{G}_2(\omega_1)S_{zo}(\omega-\omega_1).\tag{77}$$

All the other expressions derived for the background spectrum (see Sec. I A), sideband spectrum (see Sec. I B) and normalized cavity spectra (see Sec. I C) for the $\mathcal{PT}$-system (active-passive resonators) can be extended to the EP-system (passive-passive resonators) using the following transformations $\gamma\to\kappa_1$, $\chi\to\tilde{\chi}$, $\Gamma\to\tilde{\Gamma}$ and $\beta\to\tilde{\beta}$. In the following, we will give the results for the normalized cavity spectrum and the amplification factor only. The rest of the expressions can be obtained from Sec. I B-Sec. I C by making the above substitutions.

1. *Regime before the EP*

This regime is defined by $\tilde{\Gamma}=(\kappa-\kappa_1)/2>g_1$ and characterized by degenerate resonant frequencies $\tilde{\Omega}_{\pm}=\Delta$ and different damping rates $\tilde{\Gamma}_{\pm}=(\kappa+\kappa_1)/2\mp\sqrt{\tilde{\Gamma}^2-g_1^2}$. Substituting $\gamma\to-\kappa_1$ into Eq. (62), we find the normalized cavity spectrum as

$$\tilde{S}(\omega)=\tilde{G}(\omega)\left[S_a(\omega)+\frac{g^2}{\kappa^2}\tilde{c}_1\tilde{S}_{z1}(\omega)+\frac{g^2}{\kappa^2}\tilde{d}_1\tilde{S}_{z2}(\omega)\right],\tag{78}$$

where $\tilde{S}_{z1}(\omega)=\mathcal{F}\left[\tilde{f}_1(t)\mathcal{F}^{-1}[S_{zo}(\omega)]\right]$, and $\tilde{S}_{z2}(\omega)=\mathcal{F}\left[\tilde{f}_2(t)\mathcal{F}^{-1}[S_{zo}(\omega)]\right]$. Here, $\tilde{f}_1(t)$ and $\tilde{f}_2(t)$ are form factors, which can be represented by $\tilde{f}_1(t)=\exp(-\tilde{\Gamma}_-|t|+i\Delta t)$ and $\tilde{f}_2(t)=\exp(-\tilde{\Gamma}_+|t|+i\Delta t)$. Also, $\tilde{c}_1$ and $\tilde{d}_1$ can be obtained from Eqs. (41) and (42) using $\gamma\to-\kappa_1$.

In the vicinity of the phase-transition point such that $g_1\to\tilde{\Gamma}$, the normalized cavity spectrum can be re-expressed as

$$\tilde{S}(\omega)\approx\tilde{G}(\omega)[S_a(\omega)+\tilde{A}\tilde{S}_z(\omega)],\tag{79}$$

where $\tilde{S}_z(\omega)=\mathcal{F}\left[\tilde{f}(t)\mathcal{F}^{-1}[S_{zo}(\omega)]\right]$ and $\tilde{f}(t)=\exp\{-[(\kappa+\kappa_1)/2]|t|-i\Delta t\}$. Then the amplification factor becomes

$$\tilde{A}=\frac{g^2}{\kappa^2}\frac{\kappa}{\kappa+\kappa_1}\left[1+\frac{4\kappa_1}{(\kappa+\kappa_1)^2}\right].\tag{80}$$

Away from the exceptional point, Eq. (77) can be described as

$$\tilde{S}(\omega)\approx\tilde{G}(\omega)[S_a(\omega)+\frac{g^2(\kappa_1^2-\tilde{\Gamma}_+^2)}{2\kappa(\kappa+\kappa_1)\sqrt{\tilde{\Gamma}^2-g_1^2}\tilde{\Gamma}_+}\tilde{S}_{z2}(\omega)],\tag{81}$$

from which we find the amplification factor as [i.e., also from Eq. (66)]

$$\tilde{A}(g,g_1)=\frac{g^2(\kappa_1^2-\tilde{\Gamma}_+^2)}{2\kappa(\kappa+\kappa_1)\sqrt{\tilde{\Gamma}^2-g_1^2}\tilde{\Gamma}_+}. \tag{82}$$

In the weak-coupling limit $g_1\to 0$, the normalized cavity spectrum can be re-expressed as

$$\tilde{S}(\omega)\approx S_a(\omega)+\frac{g^2}{\kappa^2}\tilde{S}_{z3}(\omega), \tag{83}$$

where $\tilde{S}_{z3}(\omega)=\mathcal{F}\left[\tilde{f}(t)\mathcal{F}^{-1}[S_{zo}(\omega)]\right]$ and $\tilde{f}(t)=\exp\left(-\kappa|t|+i\Delta t\right)$.

2. *Regime after the EP*

This regime is defined by $\tilde{\Gamma}=(\kappa-\kappa_1)/2<g_1$, and characterized by nondegenerate resonant frequencies $\tilde{\Omega}_\pm=\Delta\pm\sqrt{g_1^2-\tilde{\Gamma}^2}$, and the same damping rates $\tilde{\Gamma}_\pm=(\kappa+\kappa_1)/2$. Substituting $\gamma\to-\kappa_1$ in Eq. (68), we find that the normalized cavity spectrum as

$$\tilde{S}(\omega)=\tilde{G}(\omega)\left[S_a(\omega)+\frac{g^2}{\kappa^2}\frac{\kappa\kappa_1^2}{\tilde{\Gamma}_\pm(g_1^2+\kappa\kappa_1)}\tilde{S}_{z4}(\omega)+\frac{g^2}{\kappa^2}\frac{1}{\sqrt{g_1^2-\tilde{\Gamma}^2}}\frac{\kappa(-\kappa\kappa_1+\kappa_1^2-g_1^2)}{g_1^2+\kappa\kappa_1}\tilde{S}_{z5}(\omega)\right], \tag{84}$$

where $\tilde{S}_{z4}(\omega)=\mathcal{F}\left[\tilde{f}_5(t)\mathcal{F}^{-1}[S_{zo}(\omega)]\right]$, with $\tilde{f}_5(t)=\exp(-\tilde{\Gamma}_+|t|+i\tilde{\Omega}_+t)+\exp(-\tilde{\Gamma}_-|t|+i\tilde{\Omega}_-t)$, and $\tilde{S}_{z5}(\omega)=\mathcal{F}\left[\tilde{f}_6(t)\mathcal{F}^{-1}[S_{zo}(\omega)]\right]$, with $\tilde{f}_6(t)=i\mathrm{sgn}(t)\exp(-\tilde{\Gamma}_\pm|t|-i\tilde{\Omega}_+t)+i\mathrm{sgn}(t)\exp(-\tilde{\Gamma}_\pm|t|-i\tilde{\Omega}_-t)$.

In the vicinity of the phase-transition point $g_1\to\tilde{\Gamma}$, we find

$$\lim_{g_1\to\tilde{\Gamma}}\tilde{S}(\omega)=\tilde{G}(\omega)\left[\tilde{S}_a(\omega)+\frac{g^2}{\kappa^2}\frac{8\kappa^2}{(\kappa+\kappa_1)^3}\tilde{S}_{z6}(\omega)\right]=\tilde{G}(\omega)\left[\tilde{S}_a(\omega)+\frac{8g^2}{(\kappa+\kappa_1)^3}\tilde{S}_{z6}(\omega)\right]. \tag{85}$$

where $\tilde{S}_{z6}(\omega)=\mathcal{F}\left[\tilde{f}(t)\mathcal{F}^{-1}[S_{zo}(\omega)]\right]$ and $\tilde{f}(t)=\exp(-\tilde{\Gamma}_\pm|t|-i\Delta t)$. Then, the amplification factor is given by

$$\tilde{A}(g)=\frac{8g^2}{(\kappa+\kappa_1)^3} \tag{86}$$

which decreases as the total loss of the system $(\kappa+\kappa_1)$ increases, implying that the smaller the total loss, the higher the amplification.

In this regime, but far away from the exceptional point, the normalized cavity spectrum can be written as

$$\tilde{S}(\omega)=\tilde{G}(\omega)\left[\tilde{S}_a(\omega)+\frac{g^2}{\kappa^2}\frac{2}{\kappa+\kappa_1}\frac{\kappa\kappa_1^2}{g_1^2+\kappa\kappa_1}\tilde{S}_{z4}(\omega)\right]. \tag{87}$$

Then the amplification factor is given by

$$\tilde{A}(g,g_1)=\frac{g^2}{\kappa^2}\frac{2}{\kappa+\kappa_1}\frac{\kappa\kappa_1^2}{g_1^2+\kappa\kappa_1}=\frac{2g^2\kappa_1^2}{\kappa(\kappa+\kappa_1)}\frac{1}{g_1^2+\kappa\kappa_1}. \tag{88}$$

Note that $\tilde{A}(g,g_1)$ can be made very high by decreasing κ or by increasing the coupling strength g of the optical modes.

Finally, in the very strong coupling limit $g_1\to\infty$, we find, using Eqs. (37) and (60) that

$$\tilde{S}(\omega)=0, \tag{89}$$

and obviously there is no amplification.

In Figs. 2a and 2b, we present the amplification factor $\tilde{A}(g_1,g)$ as a function of the normalized coupling strength $g_1/\tilde{\Gamma}$ for the two-lossy cavities system at two different loss ratios κ_1/κ. It is clearly seen that in the vicinity of the EP,

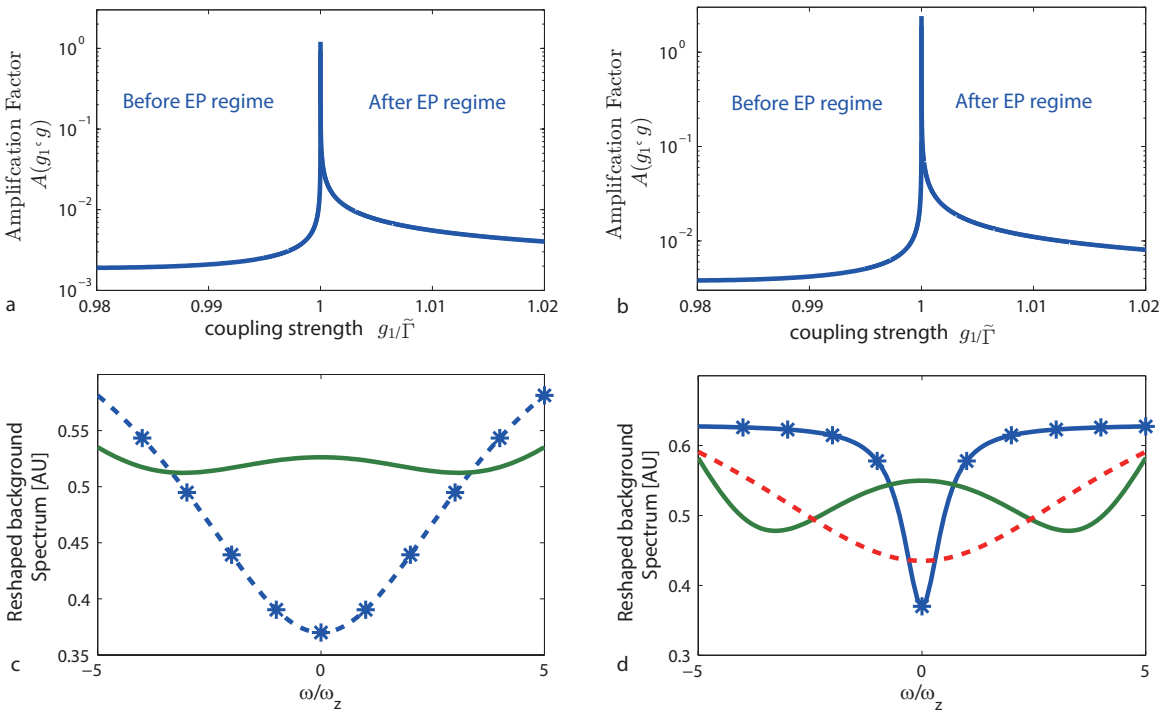

FIG. 2: (Color online) (a,b) Amplification factor $\tilde{A}(g_1, g)$ of the backaction spectrum versus the normalized coupling strength $g_1/\tilde{\Gamma}$ between the cavity and the system being measured with $\kappa = 20$MHz and $\omega_z = 6$MHz when (a) $\kappa_1 = 16$MHz (i.e., loss ratio $\kappa_1/\kappa = 0.8$) and (b) $\kappa_1 = 0.2$MHz (i.e., loss ratio $\kappa_1/\kappa = 0.01$). There is a 2-fold increase in the maximum value of $\tilde{A}(g_1, g)$ when κ_1/κ is decreased from its value of 0.8 in (a) to 0.01 in (b). (c,d) Normalized background spectrum $S_a(\omega)$ of a single-cavity system (red dashed curve), and of the two-lossy-cavity system in the regime after the EP (green curve) and in the regime before the EP(blue curve with stars) at $\omega_z = 6$MHz and $\kappa = 20$MHz when (c) $\kappa_1 = 16$MHz (i.e., $\kappa_1/\kappa = 0.8$), and (d) $\kappa_1 = 0.2$MHz (i.e., $\kappa_1/\kappa = 0.01$). Before the EP, the background spectrum shows splitting, and the split modes become more apparent as the κ_1/κ decreases. When the loss ratio κ_1/κ is large the spectrum of the two-lossy-cavity system is nearly the same as the spectrum of the single-cavity system (c). When κ_1/κ is very small, the spectrum after the EP is narrower (d).

$\tilde{A}(g_1, g)$ takes its maximum value, and it reaches higher values as κ_1/κ approaches to zero (i.e., when the difference in the losses of the cavities is very large). A decrease from $\kappa_1/\kappa = 0.8$ to $\kappa_1/\kappa = 0.01$ leads to a 2-fold increase from $\tilde{A}(g_1, g) = 1$ to $\tilde{A}(g_1, g) = 2$. Moreover, as we approach to (move away from) the EP, the change in $\tilde{A}(g_1, g)$ is sharper in the regime before the EP than in the regime after the EP. Therefore, in the regions away from the EP, $\tilde{A}(g_1, g)$ has higher values in the regime after the EP than in the regime before the EP.

Figures 2c and 2d depict the normalized background spectra $S_a(\omega)$ of the two-lossy-cavity system in the regime before and after the EP in comparison with the spectra of a single-cavity system for two different loss ratios κ_1/κ. As expected in the regime before the EP, the spectra show mode splitting. In the regime after the EP, the modes coalesce and there is only one resonant dip. Compared to the single-cavity system composed of only one passive (with loss) resonator, the two-cavity system in the regime after the EP has a narrower spectrum if the loss ratio κ_1/κ of the cavities is very small (i.e., the cavities have a significant difference in the amount of losses they have).

B. Non-zero frequency detuning

Here we consider the case of coupled modes with non-zero frequency detuning. Comparing with Eq. (74), the non-Hermitian Hamiltonian of this system is described by

$$H = (\Delta_1 - i\kappa)\, a^\dagger a + (\Delta_2 - i\kappa_1)\, c^\dagger c + g_1(a^\dagger c + c^\dagger a) + g a^\dagger a z, \tag{90}$$

where $\Delta_1 - \Delta_2 = \Delta_c$. Without the interaction term $g a^\dagger a z$, Eq. (90) accounts for the coupling between the optical modes of the microcavities and leads to two supermodes $a_\pm$ that are described with the complex frequencies

$$\omega_\pm = \frac{\Delta_1 + \Delta_2}{2} - i\frac{\kappa + \kappa_1}{2} \mp \tilde{\tilde{\beta}}, \tag{91}$$

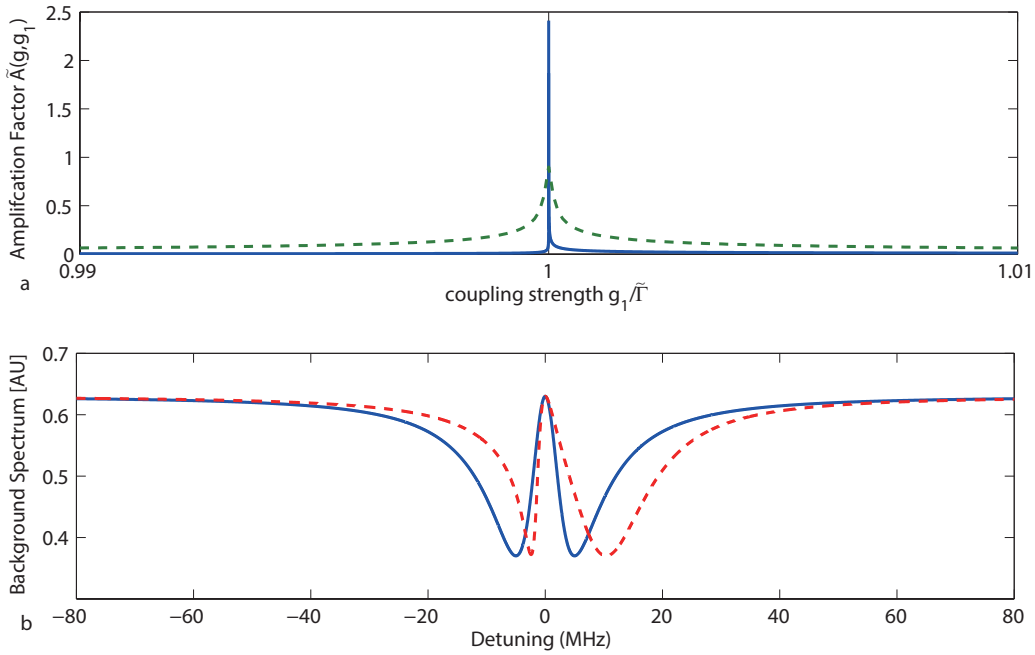

FIG. 3: (Color online)(a) Amplification factor $\tilde{A}(g, g_1)$ versus coupling strength with $\Delta_c = 0$ MHz (blue curve), $\Delta_c = 0.01$ MHz (green dashed curve). (b) Normalized background spectra of the two coupled lossy cavities versus detuning with $\Delta_c = 0$ MHz (blue curve) and $\Delta_c = 5$ MHz (red dashed curve) under the coupling strength $g_1 = 5$ MHz. The values of the parameters used in the simulations are: $\kappa = 10$ MHz and $\kappa_1 = 0.01$ MHz (i.e., $\kappa_1/\kappa = 0.001$)

where $\tilde{\tilde{\beta}} = \sqrt{g_1^2 + \Delta_c^2/4 - i\Delta_c(\kappa - \kappa_1) - (\kappa - \kappa_1)^2/4}$. In an EP system (lossy coupled modes) where there is zero-detuning between the modes, we have $\tilde{\beta} = \sqrt{g_1^2 - (\kappa - \kappa_1)^2/4}$, which becomes zero exactly at the EP. Clearly, $\tilde{\tilde{\beta}}$, obtained for non-zero detuning between the modes, cannot be made zero. Thus, the amplification seen at the EP point cannot be attained for the non-zero detuning case (Fig 2a,b).

Assuming very small detuning Δ_c, the normalized cavity spectrum can be re-expressed as

$$\tilde{S}(\omega) \approx \tilde{G}(\omega)[S_a(\omega) + \tilde{A}(g, g_1)\tilde{S}_z(\omega)], \tag{92}$$

where $S_a(\omega)$ is the background spectrum; and $\tilde{A}(g, g_1)$ is the amplification factor. Figure 3a depicts the amplification factor as a function of $g_1/\tilde{\Gamma}$, where $\tilde{\Gamma} = (\kappa - \kappa_1)/2$, for various values of Δ_c. It is clearly seen that as the detuning Δ_c increases, the amplification factor decreases. As shown in Fig 3b, when the resonant modes of the microresonators have non-zero frequency-detuning with $\kappa_1/\kappa = 0.001$, the spectrum exhibits asymmetric Fano resonances due to the coupling between the high- and low-Q modes. At zero detuning, as shown in Fig 3b, there is a transparency window originated from Fano interferences [4]. As Δ_c increases, the asymmetry in the spectrum becomes much clearer (red dashed curve in Fig 3b), and the difference of the linewidths of the modes becomes clearer. The mode with narrower linewidth will be beneficial to metrology and sensing.

The square-root topology EP (and $\mathcal{PT}$-symmetric) systems affect their scattering matrices in such a way that the coalescence of two resonance modes (each described by a single pole of the scattering matrix of the system) at an EP (or a $\mathcal{PT}$-transition point) a pole of second order emerges besides the usual first order pole. The interference of these poles leads to asymmetric lineshape profiles that have been shown to be described as genuine Fano resonances [5–7], which have been observed in many physical systems (due to the coupling of a low- and a high-Q mode) and used for high-performance sensing enabled by their sharp spectral response and high field enhancement [8, 9]. This suggests a similarity of the underlying physics of sensitivity enhancement between Fano systems and EP systems in the vicinity of an EP (or $\mathcal{PT}$-transition); however, it is still unclear whether all resonances that can be fit by the Fano formula have their origin in an EP.

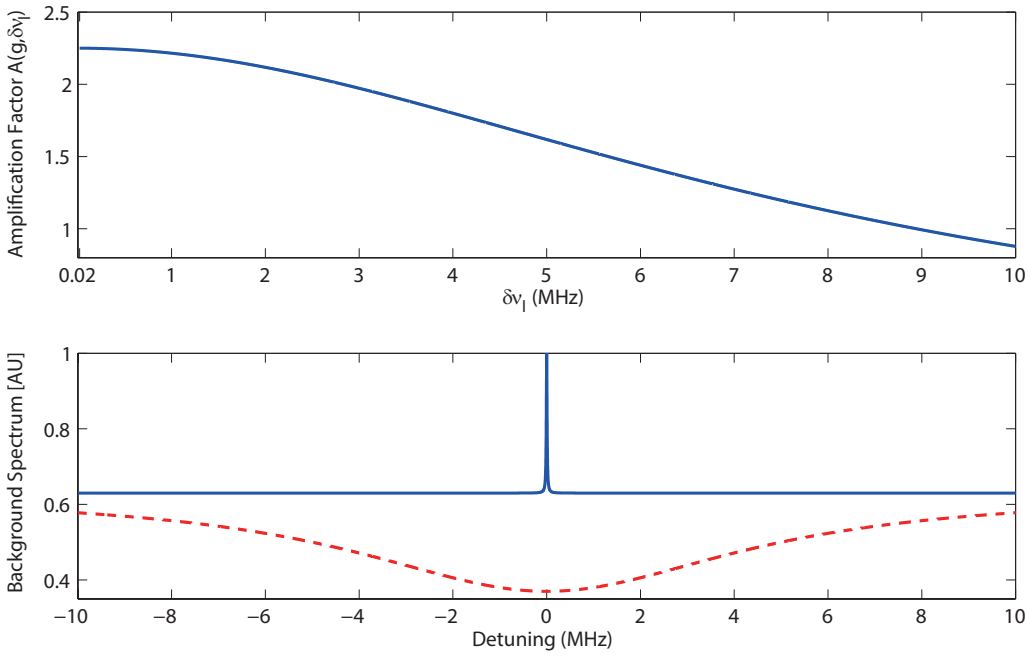

FIG. 4: (Color online)(a) Amplification factor $A(g, \delta\nu_l)$ versus linewidth of the laser coupled to the mechanical mode. (b) Normalized background spectra versus detuning for the active-cavity transducer (blue curve) and single lossy-cavity transducer (red dashed curve), with the values of the parameters used in the simulations: $\delta\nu_l = 20$ KHz and $\kappa = 10$ MHz.

III. AMPLIFICATION IN A SYSTEM WITH AN ACTIVE CAVITY

The fundamental linewidth $\delta\nu_l$ of a laser is given by the Schawlow-Townes limit [10] as

$$\delta\nu_l = \frac{\pi h\nu(\delta\nu)^2}{P_{\text{out}}}, \tag{93}$$

where $h\nu$ is the photon energy with h representing the Plank's constant and ν denoting the cavity resonant frequency; $\delta\nu$ is the cold cavity (i.e., when gain medium is not excited) resonant linewidth that is related to the cold cavity Q through $\delta\nu = \nu/Q$; P_{out} is the laser output power. The spectrum of the laser is Lorentzian, and thus can be expressed as

$$S(\omega) = \frac{2\delta\nu_l}{\delta\nu_l^2 + (\omega - \Delta)^2}, \tag{94}$$

where Δ is the detuning frequency of the laser cavity. If the laser cavity couples to a mechanical system, the normalizd spectrum can be written as

$$S(\omega) \approx G(\omega)[S_a(\omega) + A(g, \delta\nu_l)S_b(\omega)], \tag{95}$$

where $G(\omega) \equiv 1$ in the single-cavity system; $S_a(\omega)$ is the spectrum of the laser cavity; $S_b(\omega)$ is the spectrum of the mechanical mode with $S_b(\omega) = (\delta\nu_l + \gamma_m)/((\omega - \Delta - \omega_m)^2 + (\gamma_m + \delta\nu_l)^2)$; $A(g, \delta\nu_l)$ is an amplification factor given by $A(g, \delta\nu_l) = g^2/((\omega_m - \Delta)^2 + \delta\nu_l^2)$; g is the coupling strength between the optical mode and the mechanical mode; ω_m is the frequency of the mechanical mode; and γ_m is the decay rate of the mechanical mode. As the linewidth increases, the amplification factor $A(g, \delta\nu_l)$ decreases slightly, as seen in Fig 4a. Moreover, we can find due to the presence of the gain, the linewidth of the background spectrum for the active-cavity transducer is narrower than that for the passive-cavity optomechanical transducer, as shown in Fig 4b.

FIG. 5: (Color online) (a,b) Output spectra of the optomechanical transducers versus normalized frequency ω/ω_m. (c,d) Normalized susceptibility coefficient $G(\omega)$ versus normalized frequency ω/ω_m. The values of the parameters used in the simulations are: $\Delta = 0$ MHz, $\omega_m = 6$ MHz, $\kappa = 20$ MHz, $\gamma_m = 0.2$ MHz and $g = 5$ MHz, with γ taking the values of $\gamma = 16$ MHz (i.e., $\gamma/\kappa = 0.8$) in (a,c), and $\gamma = 19.98$ MHz (i.e., $\gamma/\kappa = 0.999$) in (b,d).

IV. CALCULATIONS OF THE PHONON SIDEBANDS

In our $\mathcal{PT}$ metrology system, the effective decay rate is greatly decreased by the presence of the gain. Here we will calculate the phonon sidebands [13–16] taking the gain into account. As an example, we calculate the spectrum up to the second-order term in Eq. (17). In the optomechanical system we consider here, the general measurement backaction spectrum $S_z(\omega)$ is taken as the spectrum $S_b(\omega)$ of the mechanical mode. In the broken-$\mathcal{PT}$ regime, we have

$$\begin{aligned} & \int_{-\infty}^{+\infty}\int_{-\infty}^{+\infty} \mathrm{d}\omega_1 \mathrm{d}\omega_2 G_1(\omega_1) G_2(\omega_2) S_b(\omega_2-\omega_1) S_b(\omega-\omega_1) \\ \approx\ & c_2 \frac{\Gamma_{a2}}{(\omega-\Delta-2\omega_m)^2+\Gamma_{a2}^2} + d_2 \frac{\Gamma_{b2}}{(\omega-\Delta-2\omega_m)^2+\Gamma_{b2}^2}, \end{aligned} \tag{96}$$

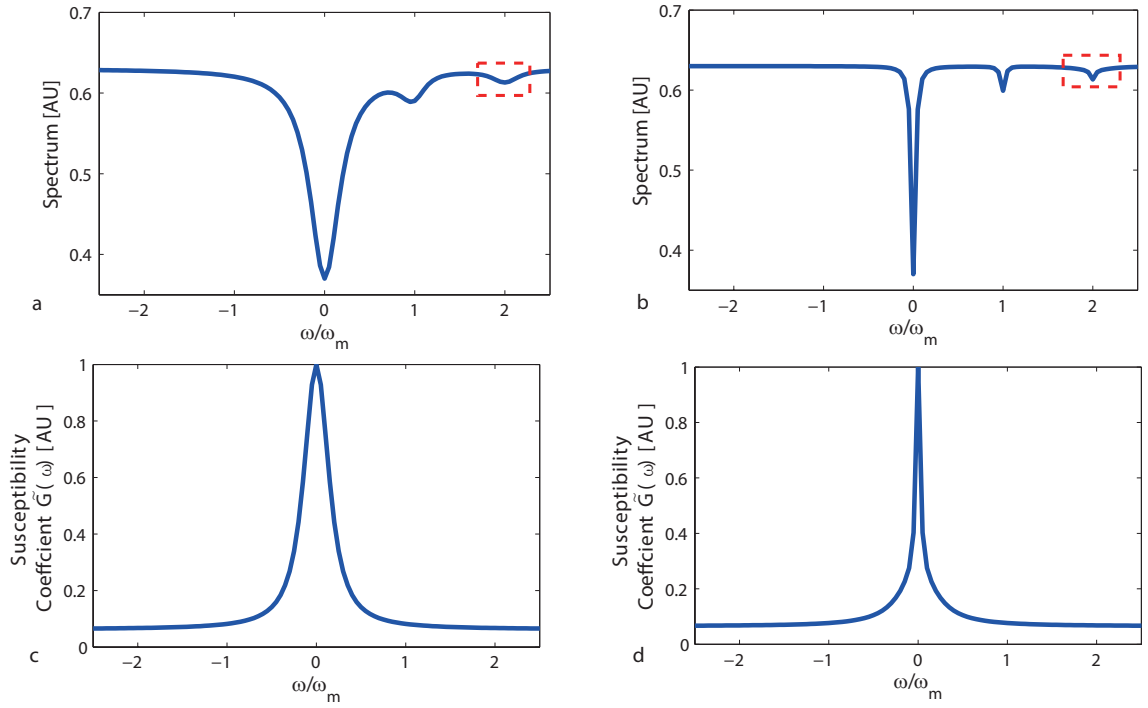

FIG. 6: (Color online) (a,b) Output spectra of the optomechanical transducers with two lossy cavities versus normalized frequency ω/ω_m. (c,d) Normalized susceptibility coefficient $\tilde{G}(\omega)$ versus normalized frequency ω/ω_m. The values of the parameters used in the simulations are: $\Delta = 0$ MHz, $\omega_m = 30$ MHz, $\kappa = 10$ MHz, $\gamma_m = 1$ MHz and $g = 6$ MHz, with κ_1 taking the values of $\kappa_1 = 8$ MHz (i.e., $\kappa_1/\kappa = 0.8$) in (a,c), and $\kappa_1 = 0.1$ MHz (i.e., $\kappa_1/\kappa = 0.01$) in (b,d).

where

$$
\begin{aligned}
S_b &= \frac{\gamma_m}{(\omega-\omega_m)^2+\gamma_m^2}, \\
c_2 &= c_1 \frac{g^2(\Gamma_-^2-\gamma^2)}{(\kappa-\gamma)\Gamma_-\sqrt{\Gamma^2-g_1^2}(\Gamma_-+\Gamma_++\gamma_m)}, \\
d_2 &= d_1 \frac{g^2(\gamma^2-\Gamma_+^2)}{(\kappa-\gamma)\Gamma_+\sqrt{\Gamma^2-g_1^2}(\Gamma_-+\Gamma_++\gamma_m)},
\end{aligned}
$$

and $\gamma_{a2} = 2\gamma_m + \Gamma_+$, $\gamma_{b2} = 2\gamma_m + \Gamma_-$. Including the high-order terms, the spectrum $S(\omega)$ can be expressed as

$$
S(\omega) \approx \sum_{n=1}^{\infty} c_n \frac{\Gamma_{an}}{(\omega-\Delta-n\omega_m)^2+\Gamma_{an}^2} + \sum_{n=1}^{\infty} d_n \frac{\Gamma_{bn}}{(\omega-\Delta-n\omega_m)^2+\Gamma_{bn}^2}. \tag{97}
$$

Figure 5 shows the results of the numerical simulations of the spectrum $S(\omega)$ for the $\mathcal{PT}$ optomechanical systems. Phonon sidebands up to the second order term is clearly seen. The first sideband is located at the mechanical frequency ω_m and the second sideband is at $2\omega_m$. The spectrum is dependent on the susceptibility coefficient $G(\omega)$. When the system is more balanced (i.e., gain-to-loss ratio is close to one), the second sideband becomes much clearer because $G(\omega)$ becomes narrower and is shifted above the zero level.

In Figure 6, we show the results of the numerical simulations of the spectrum $\tilde{S}(\omega)$ when the transducer is built from two lossy cavities (i.e., passive cavity; no active cavity). The phonon sidebands are unresolved in the bad-cavity regime, i.e. $\omega_m < \kappa$, which is irrelevant to the optomechanical coupling strength [13–16]. In the resolved sideband regime $\omega_m \gg \kappa$, we can observe phonon sidebands up to second order. The first sideband is located at the mechanical frequency ω_m and the second sideband is at $2\omega_m$. The spectrum can be affected by the susceptibility coefficient $\tilde{G}(\omega)$. When the two damping rates κ and κ_1 are very different, i.e. $\kappa \gg \kappa_1$, the sidebands become much clearer because $\tilde{G}(\omega)$ becomes narrower.

In Figure 7, we show the results of the numerical simulation of the spectrum $S_g(\omega)$ when the transducer is built from an active cavity. The phonon sidebands are unresolved in the bad-cavity regime, i.e. $\omega_m < \delta\nu_l$. In the regime

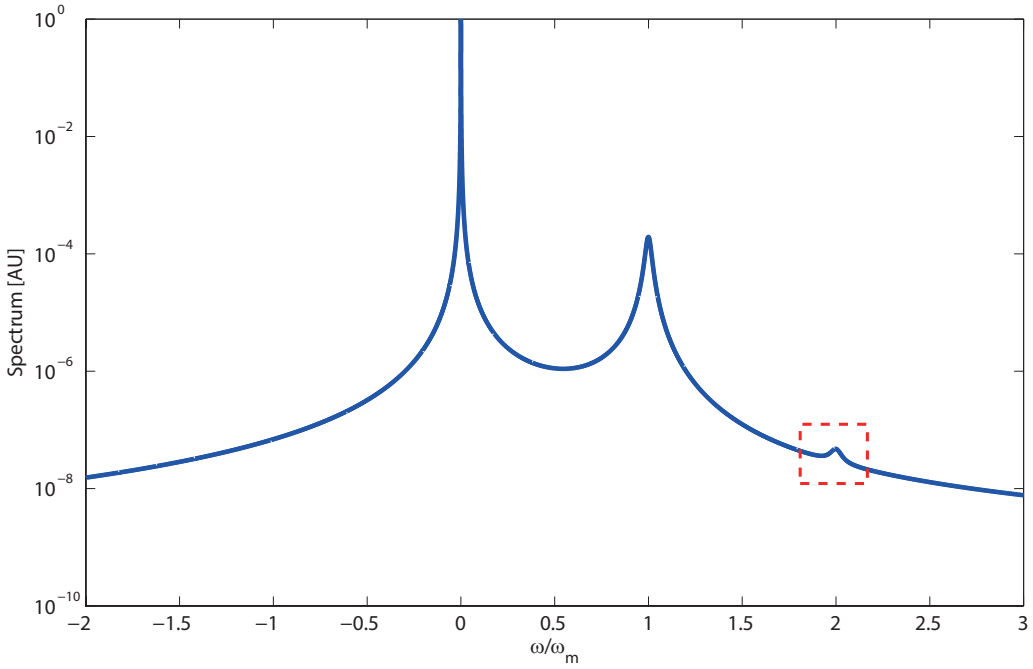

FIG. 7: (Color online) Normalized output spectra of the active-cavity optomechanical-transducer versus normalized frequency ω/ω_m. The values of the parameters used in the simulations are: $\Delta = 0$ MHz, $\omega_m = 30$ MHz, $\gamma_m = 1$ MHz and $g = 6$ MHz, and active cavity linewidth $\delta\nu_l = 20$ kHz.

$\omega_m \gg \delta\nu_l$, we observe phonon sidebands up to the second order. The first sideband is located at the mechanical frequency ω_m and the second sideband is at $2\omega_m$. Since the coupling strength between the optical mode and the mechanical mode cannot be significantly enhanced just by the presence of gain (i.e., active cavity), the observation of the sidebands relies on whether the cavity mode has sufficiently narrower linewidth or not.

V. DISPLACEMENT SPECTRAL DENSITIES IN THE ACTIVE CAVITY, $\mathcal{PT}$ AND EP OPTOMECHANICAL TRANSDUCER

The standard quantum limit of the optomechanical transducer can be characterized by the displacement spectral density and the quantum backaction force spectral density. The displacement spectral density $S_{\rm xx,single}(\omega)$ and the quantum backaction force spectral density $S_{\rm FF,single}(\omega)$ for a single cavity transducer are given by [11]:

$$S_{\rm xx,single}(\omega) = \frac{\kappa^2\hbar\omega_c}{64g^2P_{\rm in}}\left(1+\frac{4\omega}{\kappa^2}\right), \tag{98}$$

$$S_{\rm FF,single}(\omega) = \frac{16\hbar g^2P_{\rm in}}{\kappa^2\omega_c}\left(1+\frac{4\omega}{\kappa^2}\right)^{-1}, \tag{99}$$

where $P_{\rm in}$ is the input power; κ is the decay rate of the optical cavity; and ω_c is the frequency of the optical cavity. Then, for an active-cavity optomechanical transducer, the displacement spectral density $S_{\rm xx,gain}(\omega)$ and the quantum backaction force spectral density $S_{\rm FF,gain}(\omega)$ are expressed as

$$S_{\rm xx,gain}(\omega) = \frac{\delta\nu_l^2\hbar\omega_c}{64g^2P_{\rm in}}\left(1+\frac{4\omega}{\delta\nu_l^2}\right), \tag{100}$$

$$S_{\rm FF,gain}(\omega) = \frac{16\hbar g^2P_{\rm in}}{\delta\nu_l^2\omega_c}\left(1+\frac{4\omega}{\delta\nu_l^2}\right)^{-1}, \tag{101}$$

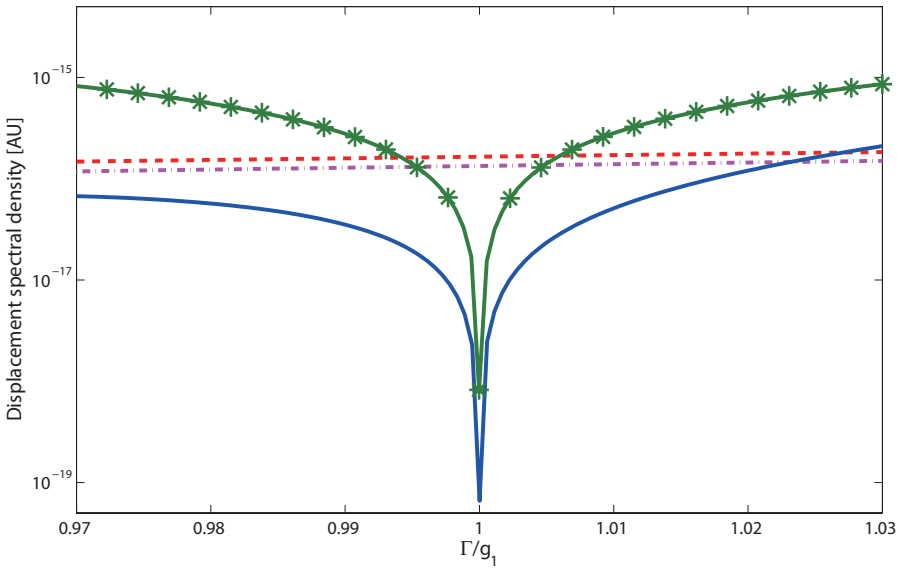

FIG. 8: (Color online) The normalized displacement spectral densities $S_{\rm xx,single}(\omega_m)$, $S_{\rm xx,gain}(\omega_m)$ $S_{\rm xx,PT}(\omega_m)$ and $S_{\rm xx,EP}(\omega_m)$ of the single cavity-optomechanical transducer (red curve) , the single active cavity transducer (pink dotted curve), the $\mathcal{PT}$-optomechanical transducer (blue curve) and the two-lossy-cavity transducer (green curve with star marks) when $\omega_m/\kappa = 0.3$. The measurement sensitivity of single active-cavity transducer is larger than the one of single passive-cavity transducer due to the narrower linewidth. Here we set the active cavity linewidth as 20 KHz. While the coupling strength of the optical mode and the mechanical mode cannot be enhanced by a single-cavity with gain, the measurement sensitivity of single cavity with gain transducer is less than the EP transducer or $\mathcal{PT}$ transducer. The measurement sensitivity is *enhanced* by at least *two* orders of magnitude by the $\mathcal{PT}$ optomechanical transducer near the transition point, i.e., $S_{\rm xx,PT}(\omega_m)/S_{\rm xx,single}(\omega_m) < 10^{-2}$, and the $\mathcal{PT}$-system performs much better than the EP-system due to the gain-loss balance of the $\mathcal{PT}$ structure.

where $\delta\nu_l$ is the linewidth of the active cavity. For the $\mathcal{PT}$ optomechanical transducer, we tune the frequency of the driving field such that the supermode a_- couples to the mechanical mode. Thus, the displacement spectral density $S_{\rm xx,PT}(\omega)$ and the quantum backaction force spectral density $S_{\rm FF,PT}(\omega)$ of the $\mathcal{PT}$ optomechanical transducer can be represented by

$$S_{\rm xx,PT}(\omega) = \frac{\Gamma_-^2\hbar\Omega_-}{64g_{\rm eff}^2P_{\rm in}}\left(1+\frac{4\omega}{\Gamma_-^2}\right), \tag{102}$$

$$S_{\rm FF,PT}(\omega) = \frac{16\hbar g_{\rm eff}^2P_{\rm in}}{\Gamma_-^2\Omega_-}\left(1+\frac{4\omega}{\Gamma_-^2}\right)^{-1}. \tag{103}$$

From Eqs. (102) and (103), we can check that $S_{\rm xx,PT}(\omega)$ and $S_{\rm FF,PT}(\omega)$ satisfy the Heisenberg inequality [12], i.e., $\sqrt{S_{\rm xx,PT}(\omega)S_{\rm FF,PT}(\omega)} \geq \hbar/2$.

We show our simulation results about the displacement spectral density in Fig. 8. As shown in Fig. 8, the displacement spectral density of the $\mathcal{PT}$-symmetric optomechanical transducer (blue curve) is minimized at the transition point. To explain this, we can see from Eq. (102) that the displacement spectral density $S_{\rm xx,PT}(\omega_m)$ increases monotonously increasing decay rate Γ_- and frequency Ω_-, while it is inversely proportional to the square of the effective cavity optomechanics (COM) coupling strength $g_{\rm eff}$. Recall that, in the $\mathcal{PT}$-breaking regime, we have $\Gamma_- = \chi + \sqrt{\Gamma^2 - g_1^2}$ and $\Omega_- = \Delta$. Thus, when we increase the inter-cavity coupling strength g_1, the decay rate Γ_- will decrease and the COM coupling strength $g_{\rm eff}$ will increase, which leads to the decrease of $S_{\rm xx,PT}(\omega)$. In the $\mathcal{PT}$-symmetric regime, we have $\Gamma_- = \chi$ and $\Omega_- = \Delta - \sqrt{g_1^2 - \Gamma^2}$. Thus, when we increase g_1, the frequency Ω_- and the COM coupling strength $g_{\rm eff}$ will decrease, which leads to the increase of $S_{\rm xx,PT}(\omega)$.

Similarly, we can calculate the displacement spectral density $S_{\rm xx,EP}(\omega)$ and the quantum backaction force spectral density $S_{\rm FF,EP}(\omega)$ of the two-lossy-cavity transducer

$$S_{\rm xx,EP}(\omega) = \frac{\tilde{\Gamma}_-^2\hbar\tilde{\Omega}_-}{64\tilde{g}_{\rm eff}^2P_{\rm in}}\left(1+\frac{4\omega}{\tilde{\Gamma}_-^2}\right), \tag{104}$$

$$S_{\mathrm{FF,EP}}(\omega)=\frac{16\hbar\tilde{g}_{\mathrm{eff}}^{2}P_{\mathrm{in}}}{\tilde{\Gamma}_{-}^{2}\tilde{\Omega}_{-}}\left(1+\frac{4\omega}{\tilde{\Gamma}_{-}^{2}}\right)^{-1}. \tag{105}$$

As shown in Fig. 8, we can observe a similar decrease of the displacement spectral density for $\mathcal{PT}$ and EP systems near the transition point, but the $\mathcal{PT}$-system performs much better because the effective damping rate of the $\mathcal{PT}$-system is much smaller due to the gain-loss balance of the $\mathcal{PT}$-symmetric structure.

[1] C. M. Bender, D. C. Brody, and H. F. Jones, Complex extension of quantum mechanics, Phys. Rev. Lett. **89**, 270401 (2002).
[2] C. M. Bender, D. C. Brody, H. F. Jones, and B. K. Meister, Faster than Hermitian quantum mechanics, Phys. Rev. Lett. **98**, 040403 (2007).
[3] J. Stein, in *Digital Signal Processing: A Computer Science Perspective*, edited by J. G. Proakis (Wiley, 2000), p. 115.
[4] B. Peng, Ş. K. Özdemir, W. Chen, F. Nori and L. Yang, What is and what is not electromagnetically induced transparency in whispering-gallery microcavities, Nat. Comm. **5**, 5082 (2014).
[5] L. Schwarz, H. Cartarius, G. Wunner, W. D. Heiss and J. Main, Fano resonances in scattering: an alternative perspective, Eur. Phys. J. D **69**, 196 (2015).
[6] W. D. Heiss and G. Wunner, Fano-Feshbach resonances in two-channel scattering around exceptional points, Eur. Phys. J. D **68**, 284 (2014).
[7] A. I. Magunov, I. Rotter, and S. I. Strakhova, Fano resonances in the overlapping regime, Phys. Rev. B **68**, 245305 (2003).
[8] Y. Zhang, Y. Zhen, O. Neumann, J. K. Day, P. Nordlander, N. J. Halas, Coherent anti-Stokes Raman scattering with single-molecule sensitivity using a plasmonic Fano resonance, Nat. Comm. **5**, 4424 (2014).
[9] A. K. Dmitry, P. Zhenying, I. K. Arseniy and A. K. Leonid, Quantum spectroscopy of plasmonic nanostructures, Phy. Rev. X **4**, 011049 (2014).
[10] A. Schawlow, and C. Townes, Infrared and optical masers. Phys. Rev. **112**, 1940-1949 (1958).
[11] J. M. Dobrindt and T. J. Kippenberg, Theoretical analysis of mechanical displacement measurement using a multiple cavity mode transducer, Phys. Rev. Lett. **104**, 033901 (2010).
[12] V. B. Braginsky and F. Khalili, *Quantum measurement* (Cambridge University Press, Cambridge, England, 1992).
[13] P. Rabl, Photon blockade effect in optomechanical systems, Phys. Rev. Lett. **107**, 063601 (2011).
[14] A. Nunnenkamp, K. Børkje, and S. M. Girvin, Single-Photon Optomechanics, Phys. Rev. Lett. **107**, 063602 (2011).
[15] J.-Q. Liao, H. K. Cheung, and C. K. Law, Spectrum of single-photon emission and scattering in cavity optomechanics, Phys. Rev. A **85**, 025803 (2012).
[16] X.-W. Xu, Y. J. Li, and Y. X. Liu, Photon-induced tunneling in optomechanical systems, Phys. Rev. A **87**, 025803 (2013).